CANADIAN THESES ON MICROFICHE

I.S.B.N.

THESES CANADIENNES SUR MICROFICHE

National Library of Canada
Collections Development Branch

Canadian Theses on
Microfiche Service

Ottawa, Canada
K1A 0N4

Bibliothèque nationale du Canada
Direction du développement des collections

Service des thèses canadiennes
sur microfiche

NOTICE

The quality of this microfiche is heavily dependent upon the quality of the original thesis submitted for microfilming. Every effort has been made to ensure the highest quality of reproduction possible.

If pages are missing, contact the university which granted the degree.

Some pages may have indistinct print especially if the original pages were typed with a poor typewriter ribbon or if the university sent us a poor photocopy.

Previously copyrighted materials (journal articles, published tests, etc.) are not filmed.

Reproduction in full or in part of this film is governed by the Canadian Copyright Act, R.S.C. 1970, c. C-30. Please read the authorization forms which accompany this thesis.

THIS DISSERTATION
HAS BEEN MICROFILMED
EXACTLY AS RECEIVED

AVIS

La qualité de cette microfiche dépend grandement de la qualité de la thèse soumise au microfilmage. Nous avons tout fait pour assurer une qualité supérieure de reproduction.

S'il manque des pages, veuillez communiquer avec l'université qui a conféré le grade.

La qualité d'impression de certaines pages peut laisser à désirer, surtout si les pages originales ont été dactylographiées à l'aide d'un ruban usé ou si l'université nous a fait parvenir une photocopie de mauvaise qualité.

Les documents qui font déjà l'objet d'un droit d'auteur (articles de revue, examens publiés, etc.) ne sont pas microfilmés.

La reproduction, même partielle, de ce microfilm est soumise à la Loi canadienne sur le droit d'auteur, SRC 1970, c. C-30. Veuillez prendre connaissance des formules d'autorisation qui accompagnent cette thèse.

LA THÈSE A ÉTÉ
MICROFILMÉE TELLE QUE
NOUS L'AVONS REÇUE

NL-339 (r. 82/08)

Canada

1

0-315-15911-1

National Library of Canada
Canadian Theses Division
Ottawa, Canada
K1A 0N4

Bibliothèque nationale du Canada
Division des thèses canadiennes

63820

PERMISSION TO MICROFILM — AUTORISATION DE MICROFILMER

• Please print or type — Écrire en lettres moulées ou dactylographier

Full Name of Author — Nom complet de l'auteur

DAVID J PRIDIC

Date of Birth — Date de naissance

11 JUN 54

Country of Birth — Lieu de naissance

CANADA.

Permanent Address — Résidence fixe

302 8503 99 St
EDM. ALTA
T6E 3T7.

Title of Thesis — Titre de la thèse

A STUDY OF THE CHARPY TEST

University — Université

UNIVERSITY OF ALTA.

Degree for which thesis was presented — Grade pour lequel cette thèse fut présentée

M.Sc.

Year this degree conferred — Année d'obtention de ce grade

1983

Name of Supervisor — Nom du directeur de thèse

DR. D G BELLOW

Permission is hereby granted to the NATIONAL LIBRARY OF CANADA to microfilm this thesis and to lend or sell copies of the film.

The author reserves other publication rights, and neither the thesis nor extensive extracts from it may be printed or otherwise reproduced without the author's written permission.

L'autorisation est, par la présente, accordée à la BIBLIOTHÈQUE NATIONALE DU CANADA de microfilmer cette thèse et de prêter ou de vendre des exemplaires du film.

L'auteur se réserve les autres droits de publication; ni la thèse ni de longs extraits de celle-ci ne doivent être imprimés ou autrement reproduits sans l'autorisation écrite de l'auteur.

APR 18 1983.

Date

Signature

NL-91 (4/77)

THE UNIVERSITY OF ALBERTA

A STUDY OF THE CHARPY TEST

by

(C) DAVID J. PRIDIE

A THESIS

SUBMITTED TO THE FACULTY OF GRADUATE STUDIES AND RESEARCH

IN PARTIAL FULFILMENT OF THE REQUIREMENTS FOR THE DEGREE

OF MASTER OF SCIENCE

DEPARTMENT OF MECHANICAL ENGINEERING

EDMONTON, ALBERTA

SPRING, 1983

THE UNIVERSITY OF ALBERTA

RELEASE FORM

NAME OF AUTHOR David J. Pridie

TITLE OF THESIS A Study of the Charpy Test

DEGREE FOR WHICH THESIS WAS PRESENTED Master of Science

YEAR THIS DEGREE GRANTED 1983

Permission is hereby granted to THE UNIVERSITY OF ALBERTA LIBRARY to reproduce single copies of this thesis and to lend or sell such copies for private, scholarly or scientific research purposes only.

The author reserves other publication rights, and neither the thesis nor extensive extracts from it may be printed or otherwise reproduced without the author's written permission.

David J. Pridie
#302, 8503 - 99 Street
Edmonton, Alberta
T6E 3T7

DATED
APR 18 1983

THE UNIVERSITY OF ALBERTA

FACULTY OF GRADUATE STUDIES AND RESEARCH

The undersigned certify that they have read, and recommend to the Faculty of Graduate Studies and Research, for acceptance, a thesis entitled

A STUDY OF THE CHARPY TEST

submitted by David J. Pridie

in partial fulfilment of the requirements for the degree of

Master of Science

Supervisor

April 6, 1983

DATE

TO MY WIFE

JANICE

AND TO MY PARENTS

MARJORIE AND LEO

ABSTRACT

Conventional Charpy test energies, using either regular or fatigue pre-cracked specimens, have been empirically correlated to fracture toughness parameters. The instrumented Charpy machine allows correlations to be made using the load at fracture. It also permits the calculation of K_d directly from Charpy data provided measurements are made of load, displacement and crack extension during impact.

Pertinent correlations in the literature were applied over a wide range of Charpy V-notch energy values and results were compared. Load determinations during impact were made and compared using strain gauges in the tup and an accelerometer on the side opposite the tup of a C-type pendulum. Displacement measurements using a Hall-effect transducer were evaluated. Energy, as a product of the measured load and displacement, was found to agree with that taken by conventional pendulum measurements. An attempt was made to produce a DC potential crack detector, but a capacitative effect in the system precluded successful results.

ACKNOWLEDGEMENT

The author expresses appreciation to

Mr. Al Muir for his shared expertise in mechanical matters

Mr. Terry Nord for his shared knowledge of electronics

TABLE OF CONTENTS

CHAPTER		PAGE
I.	HISTORY AND THEORY	1
PART 1	The Charpy V-Notch Test	2
PART 2	The Fracture Toughness Test	6
PART 3	CVNE - K_{Ic} Correlations	11
PART 4	The Instrumented CVN Test	13
II.	EXPERIMENTAL PROCEDURE	21
PART 1	Equipment	22
PART 2	Calibration	26
III.	RESULTS AND DISCUSSION	29
PART 1	Displacement	30
PART 2	Force: Strain Gauges and Accelerometer	35
PART 3	Comparison with Static Tests	37
IV.	ENERGY CONSIDERATIONS	40
PART 1	Recapitulation	41
PART 2	Energy Calculations	42
PART 3	K_{Ic} and K_{Id} from CVNE	44
PART 4	Twisting, Lateral Motion of Pendulum	48
V.	D.C. POTENTIAL CRACK MONITOR	50
PART 1	Introduction	51
PART 2	Theory	52
PART 3	Experimental	55
PART 4	Calibration	59
PART 5	Results	60
PART 6	Observations	63
VI.	CONCLUSIONS	65
BIBLIOGRAPHY		68
APPENDICES		73

LIST OF TABLES

TABLE		PAGE
I	Diffences Between CVN and K_{Ic} Measurements	12
II	Comparison of Static and Dynamic Load-Displacement Curves	39
III	CVNE by Various Methodologies	43
IV	K_{Ic} from CVN Data	45

LIST OF FIGURES

FIGURES		PAGE
1	A Typical CVN Machine	4
2	Transition Temperature Test Results	4
3	Variations in CVN Notching	4
4	Impact Energy Representation	17
5	Equipment Schematic	23
6	Typical Impact Displacement Plot	31
7	Displacement Curves for Increasing Energy Levels	33
8	K_{Ic} and K_{Id} from CVN Data	47
9	Variables for Theoretical Calibration	53
10	Crack Detector Equipment Schematic	56
11	Power and Sensor Lead Connections	58
12	Eight Wire Analogue	61
13	Charpy Quasi-Static Crack Calibration	61
14	Crack-Area and Load Representation of Results for CVN Impact Test	62

NOMENCLATURE

a	=	Crack Length, Crack Size, Flaw Size
a_{eff}	=	Effective Crack Length
B	=	Thickness
E	=	Young's Modulus (205×10^3 MPa)
F	=	Force
G	=	Crack Extension Force, Strain Energy Release Rate
G_c	=	Critical Crack Extension Force
J	=	J-Integral
K	=	Stress Intensity Factor
K_c	=	Plane Stress Fracture Toughness
K_{Ic}	=	Plane Strain Fracture Toughness
K_Q	=	Stress Intensity Factor (Conditional Fracture Toughness)
S	=	Span of Specimen
U	=	Potential Energy Per Unit Thickness of Specimen
W	=	Width of Specimen
w	=	Energy Absorbed During Impact
x,y,z	=	Rectangular Co-ordinates
υ	=	Poisson's Ratio
σ_y	=	Yield Stress
ρ	=	Crack Tip Radius, CVN Notch Radius

KEY WORDS

Charpy tests, Charpy V-notch, cracks, crack detection, displacement, dynamic fracture toughness, dynamic tests, fracture toughness, impact tests, instrumented charpy machine, instrumented impact test.

CHAPTER I

HISTORY AND THEORY

PART 1 - THE CHARPY V-NOTCH TEST

The mechanics of a common Charpy V-Notch (CVN) test are straightforward. The main components are a pendulum with a defined striking edge (tup), a set of supports (anvils) to position a specimen just past the nadir of the pendulum motion and a notched specimen of dimensions 10 x 10 x 55 mm (see Fig. 1). The pendulum is allowed to move unhindered through its arc and the final height recorded. Next, a specimen is placed on the anvils so that it is impacted by the pendulum on the face opposite the notch. The difference in height (Δh) achieved by the pendulum reflects the energy absorbed during the test (CVNE) and is calculated using

$$CVNE = Wt_{PEND}\, \Delta h \qquad (1)$$

Where Wt_{PEND} is the weight of the pendulum. This has been the essence of CVN testing since 1917, when Charpy and Thenard (1917) published a paper dealing with the application of the machine.

Other quantities that may be measured from the Charpy test are ductility and fracture appearance. Ductility is measured by noting either the lateral expansion (LE) of the leading (impacted) side of the specimen or the lateral contraction of the trailing (notched) side. Fracture appearance (FA) is measured in percent and relates either brittle fracture area (that characterized as flat, shiny and small faceted) or ductile area (that which is not brittle) to the total area.

A method for conducting the CVN test can be found in the American Society for Testing and Materials Standard E23-81 (ASTM 1982).

Charpy tests are conducted over a range of temperatures to determine where an appreciable change takes place in some or all of the above mentioned qualifiers as in Fig. 2. Acceptance limits are usually prescribed by the field history of the application and occur at what is defined as the transition temperature. One such level is the lower bound energy of 20 J at minimum service temperature which was based on American World War II ship failures. Another is the ascending acceptance levels of Charpy V-Notch Energy (CVNE) as ultimate tensile strength (UTS) increases, used by the ASME (1978) in their boiler and pressure vessel code. These ascending levels were generated by Gross' (1970) criterion of constant LE that, according to Gross, inherently compensated for differences in UTS of materials tested. This inherent compensation has been challenged by Puzak and Lange (1972) in the case of quenched and tempered steels.

Deviations in CVN testing occur mostly in specimen notching. One exception is the European practice of using a sharper and thinner tup. This leads to lower energy absorption by the specimen above the 50 J level (Rudolph, 1981). Another European practice is to vary the notch geometry as in Fig. 3. Results can only be compared if the tup and notch geometries are identical or proven equivalent.

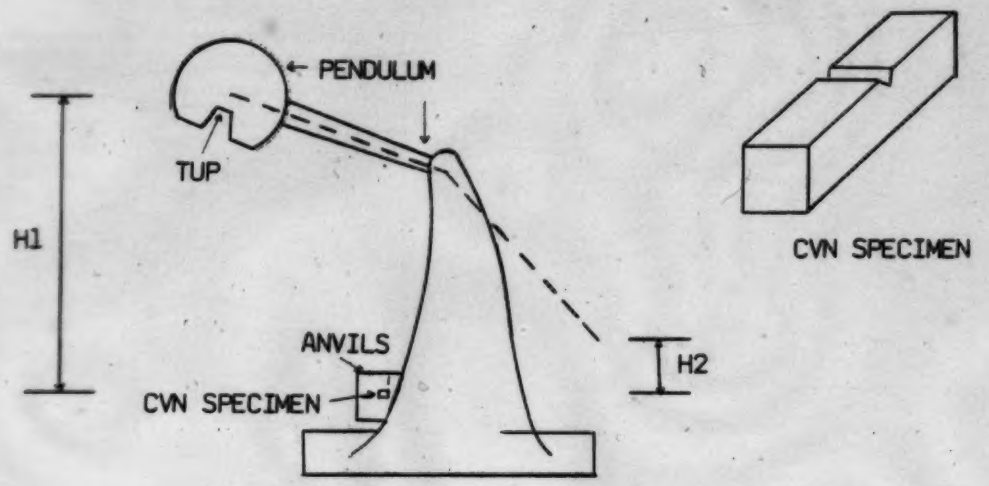

FIGURE 1. A TYPICAL CVN MACHINE

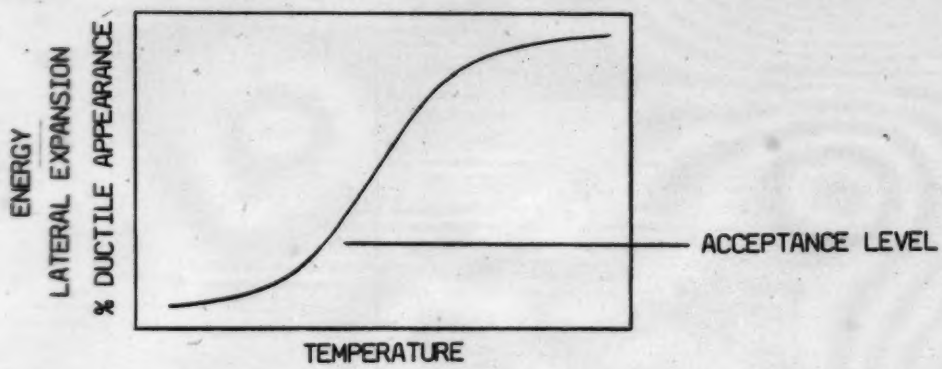

FIGURE 2. TRANSITION TEMPERATURE TEST RESULTS

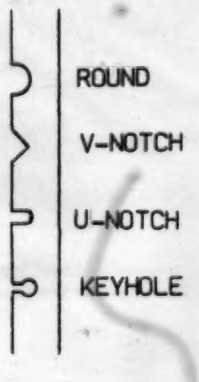

FIGURE 3. VARIATIONS IN CVN NOTCHING

(DAEVES, I.K. 1965)

The effect of notching a specimen to produce a structural discontinuity increases the tendency of a material to behave in a brittle manner. This cannot be measured by conventional unnotched tests. The severity of the notch can decrease the energy absorbed (Smith and Patchett 1975). Of considerable interest is the CVNE of specimens with fatigue induced crack fronts since the sharpness of such is considered equal to actual material flaws.

The fatigue induced crack front is the most severe of notches and reduces the energy absorbed in an impact test by increasing the stress intensity at the notch tip, and thereby decreasing the amount of plastic deformation that can take place before the onset of stable crack growth. CVNE testing requires only that the notch be of standard dimensions to promote equivalence of results between tests. If the notch itself is to be given prominence in the toughness behavior of a material, it should be of the most realistic nature; ie., fatigue induced.

PART 2 - THE FRACTURE TOUGHNESS TEST

Although Charpy testing over a range of temperatures can show transitions in brittle behaviour, the results cannot be directly applied as a design parameter. The most desired criterion is one that will allow computation of the maximum permissable flaw size in a structure under known loads. The field of fracture mechanics seeks to provide this information. The basic equation used is

$$K_c = C \sigma \sqrt{a} \qquad (2)$$

where K_c is fracture toughness, C is a constant depending on geometry, σ is the applied stress and a is the crack length.

Fracture mechanics is based on a theory by Griffith (1920, 1924) that assumes that the energy released as a crack propagates is directly proportional to the area it creates. He defined U_e as the elastic strain energy per unit thickness where

$$U_e = \pi \sigma^2 a/E$$

and U_γ as the surface free energy per unit thickness.

$$U_\gamma = 4a\gamma$$

where γ is the surface free energy per unit thickness of the material.

The condition for crack propagation was defined as

$$\partial U_e / \partial a \geq \partial U_\gamma / \partial a$$

or (solving) when

$$\sigma^2 a = 2\gamma E/\pi \qquad \text{(Plane Stress) (Conditions)} \qquad (3)$$

$$\sigma^2 a = 2\gamma E/(1-\upsilon^2)\pi \qquad \text{(Plane Strain) (Conditions)} \qquad (4)$$

which are of the form of eqn. 2. Griffith's equations were for an elliptical crack and his experiments were conducted on glass fibre and limited to materials that were linearly elastic to fracture.

Later fracture mechanics developments fell into four categories. First was the refined mathematical analysis of eqns. 3 and 4 which reasserted their validity by reproducing their form from different premises or which extended their use into the regime of plastic deformation. Second, was the development of standardized fracture toughness (FT) tests and specimen configurations. This was undertaken by the American Society for Testing and Materials to promote reproducibility between tests. Third, was the correlation of FT values to material property values such as CVNE and the fourth, was the generation of FT values for design purposes. It is not within the scope of this text to elaborate on the fourth category.

Irwin (1948) and Orowan (1949) modified Griffith's (1924) theory to account for plastic deformation at the crack tip so that eqn. 3 becomes

$$\sigma^2 a = 2E(\gamma_e + \gamma_p)/\pi \qquad \text{(Plane Stress)} \qquad (5)$$

or $$\sigma^2 \pi a/E = G \qquad \text{(Plane Stress)} \qquad (6)$$

in Irwin's notation.

Irwin (1962) used Westergaard's (1939) method in an analysis of the stress distribution along the perimeter of an elliptical crack imbedded in an infinite body subject to uniform tensile stress. He showed that the stress intensity factor in Mode I opening (where the two fracture surfaces are displaced perpendicular to one another in opposite directions) when the major axis was extended to infinity, could be written as

$$K_c = \sigma\sqrt{\pi a} \qquad \text{(Plane Stress)} \qquad (7)$$

or $$K_c^2/E = \sigma^2 \pi a/E \qquad \text{(Plane Stress).} \qquad (8)$$

Comparing eqn. 8 to eqns. 5 & 6, it can be seen that

$$K_c^2/E = \sigma^2 \pi a/E = 2(\gamma_e + \gamma_p) = G \qquad \text{(Plane Stress)}$$

where an a_{eff} is often substituted for a to compensate for the

existence of plastic deformation at the crack tip. Equations 5 through 8 are also valid for plane strain conditions when $E/(1-\upsilon^2)$ is substitued for E.

Rice (1968) used the path independent contour integral

$$J = \oint_\Gamma W dy - \vec{T} \cdot (\partial \vec{u}/\partial x)\, ds$$

to characterize the stress-strain field at a crack tip where

W = Strain energy density $= \int_0^\varepsilon \sigma_{ij} de_{ij}$

$\vec{T}$ = Traction vector $T_i = \sigma_{ij} n_{ij}$

$\vec{u}$ = Displacement vector u_i

S = Element of arc length

It can be shown that for Mode I opening and linear elastic conditions

$$J = G = K_c^2/E \qquad \text{(Plane Stress)} \qquad (9)$$

for small scale yielding. For linear or non-linear elastic materials, it can be shown that

$$J = -\partial U/\partial a \qquad (10)$$

where U is the potential energy per unit thickness.

Theoretical and experimental research into fracture mechanics parameters between 1950 and 1970 was characterized by statements on mathematical assumptions and physical restraints placed on the method. This was necessary to qualify the applications of results. The American Society for Testing and Materials has listed and defined relevant terms as part of their effort in standardizing fracture toughness testing. Appendix I contains definitions (ASTM E616 1982) of terms used here.

The American Society for Testing and Materials (ASTM) has developed a standard method for fracture toughness testing. Because of their self-imposed restrictions on reproducibility, they focused on developing a technique for the well defined static plane strain, linear elastic Mode I opening conditions (ASTM E399, 1982). Since plane strain conditions produce lower toughness values than plane stress as inferred by Rolfe and Barsom (1977), they were considered a lower bound and thus were acceptable for design purposes with errors only being on the conservative side. The scope of the test was somewhat limited because conditions were static and applied only to the initial propagation of the crack front. The problem of a running crack in metallic material where the dynamic resistance is lower, was neglected.

The mechanics of the ASTM E399 fracture toughness test are quite involved and require special testing machinery. The specimens are of intricate shape and require extensive machining. With the thickness requirement of the specimens (for plane strain conditions) only estimated and not confirmed until after the test has been performed, the process can be time consuming as well.

PART 3 - CVN-K_{Ic} CORRELATIONS

Neglecting the cost of equipment and time which is greater for performing K_{Ic} tests than for CVN tests, the cost of making a K_{Ic} specimen can be ten times that for a CVN specimen. In addition, three tests are recommended for determining fracture toughness at a reference temperature. Because of the great effort and cost required to determine the fracture toughness of a material, attempts have been made to estimate K_{Ic} from CVNE data. One application of this would be in quality control where a manufacturer could generate a correlation at the beginning of production and use the CVNE to maintain a specified level of K_{Ic} thereafter.

Although the tests are quite different, see Table I, attempts have been made to correlate K_{Ic} values to CVNE results. Sailors and Corten (1972) and Pisarski (1978) listed the prominent correlations and their application restrictions as in Appendix II.

The general form of the equations was

$$K_{Ic} \text{ or } K_{Id} = F\,(CVNE + c)^{e} \qquad (11)$$

where F and C are constants determined experimentally, and e was a positive exponent also determined by experiment.

TABLE I

DIFFERENCES BETWEEN CVN AND K_{Ic} MEASUREMENTS

(Ritchie 1978)

	CVN TEST	K_{Ic} TEST
1 Stress Concentration	Rounded Notch ($\rho \approx 0.25$ mm)	Fatigue Precrack ($\rho \rightarrow 0$)
2. Strain Rate	Impact ($\dot{\varepsilon} \approx 10^{1}$-$10^{2}$ s^{-1})	Quasi-Static ($\dot{\varepsilon} \approx 10^{-4}$ s^{-1})
3. Specimen Size	10 mm Square Rectangular	Sufficient to maintain plane strain conditions
4. Measurement Point	Crack initiation and propagation	Onset of unstable crack propagation
5. Parameter Measured	Energy absorbed by specimen	Critical value of stress intensity

Most correlations did not incorporate dimensional equivalence (units) in the constant F nor account for the differences between the tests eg., the stress concentration. Sailors and Corten (1972) noted that the relationship between K_{Ic} and CVN energy of slow bend tests were indistinguishable from those of K_{Id} and CVNE impact tests. They went further to write

$$G_{Id} = K_{Id}/E \qquad (12)$$

Ritchie (1978) showed that for an ultrahigh strength steel, increased austenizing temperatures caused an increase in K_{Ic} but a concurrent decrease in CVNE (yield strength was unaffected). This trend is in complete opposition to eqn. 11 and implies that empirical correlations developed for particular materials under restricted ranges should be used with caution.

PART 4 - THE INSTRUMENTED CHARPY V-NOTCH TEST

In order to obtain fracture toughness parameters directly from Charpy data, some modifications have to be made to the CVN test and some limitations must be accepted. Stress concentration considerations require that the specimen be fatigue precracked rather than V-notched. The high strain rate of the Charpy test limits the results to dynamic fracture toughness values K_d or K_{Id}. Since the thickness of the CVN specimen is constant at 10 mm, the categorization of dynamic fracture toughness as plane stress or plane strain depends upon the magnitude of toughness ie., the thickness requirement for the toughness level. An estimate for the minimum yield strength of a steel from which a K_{Id} value could be obtained from a Charpy size specimen is 1700 MPa (ASTM E399 1982). Thus, most steels would yield K_d values from Charpy tests. Another consideration is that side notching the CVN testpieces could induce a state of plane strain during testing and thus yield K_{Id} values.

Plati and Williams (1975) developed a method for obtaining fracture toughness values from CVNE. Their development, slightly expanded and slightly modified is outlined below.

For linear elastic fracture mechanics (LEFM) the compliance, C, is a function of crack length and geometry. Thus, for a displacement, d, and applied load, P,

$$d/P = C'(a) = C$$

since the deflection is entirely elastic, the energy, w, absorbed by the testpiece is

$$w = BUe = Pd/2 = P^2C/2 \qquad (13)$$

also under LEFM and from the eqns. 9 and 10

$$J = G = -\partial U/\partial a = dU_e/da \text{ since } Up = 0 \qquad (14)$$

thus from eqns. 13 and 14

$$G_d = dU_e/da = 1/2B\ (d(P^2C)/da) \qquad (15)$$
$$= P^2/2B\ \ (dC/da)$$

and substituting from eqn. 13

$$G_d = w/B\ \ (1/C)\ (dC/da) \qquad (16)$$

and from eqn. 12, for plane stress

$$K_d = \sqrt{EG_d} = \sqrt{Ew/B\ \ (1/C)\ (dC/da)} \qquad (17)$$

They go further to explain how to obtain experimental values for (1/C) (dC/da). They also calculate the expression and present a table of direct calibrations for Charpy test pieces.

Equation 13 and CVNE values do not necessarily generate K_d values because the restrictions of LEFM are not adhered to. Explicity CVNE measures the total energy of fracture (initiation and propagation). It is quite possible that the results of such tests would be useful as are those (G_d determinations) of Plati and Williams (1975) for polymers. However, by instrumenting the impact machine, more definite indicators can be achieved.

The addition of a force monitoring device to the Charpy apparatus allows differentiation of energy into predefined component parts much the same as with static bend tests. Initial and final velocities of the pendulum can be calculated and the average taken so that for constant acceleration

$$d = \int_0^t V dt = V_i t - 1/2\ (V_i - V_f) t^2 \qquad (18)$$

can be approximated by

$$d = \int_0^t V dt = V_{av} \int_0^t dt = V_{av} t \qquad (19)$$

with total displacement over the impact time being correct and intermediate points approaching the linear approximation (eqn. 19) as $V_f \rightarrow V_i$.

With force and displacement, it is possible to construct an energy diagram for the CVN test. Fig. 4 shows a representation of a Charpy test with characteristics identified by Kotilaingen and Sirkkola (1981) and Rawers and McMullen (1980). By choosing an appropriate portion of the total energy, K_d can be evaluated. Conditions of linear elasticity were imposed in the derivation of eqn. 17.

The stress intensity in three point bending for a precracked specimen can be calculated using methods obtained in the standard ASTM E399 (1982) by

$$K = PS/B\,(1/W^{3/2})\,f(a/w)$$

with suitable a_{eff} replacing a for other than plane strain conditions. With P measured directly, $K_Q = K$ may be generated.

Another addition to the Charpy apparatus is a displacement transducer. Calculated displacements usually assume some premise; eg., eqn. 18 assumes constant acceleration and eqn. 19 assumes constant velocity. Physical measurement of displacement avoids these assumptions. Eqn. 19 is modifed to

$$d = \int_0^t (dx/dt)\,dt$$

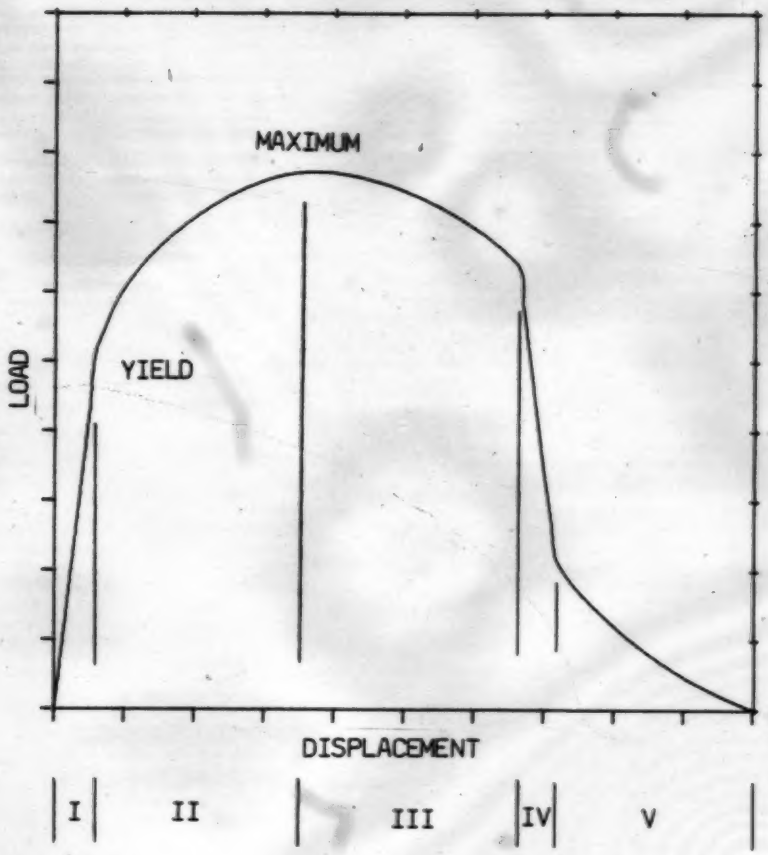

I - ELASTIC OR INITIATION

II - PLASTIC OR INITIATION-(CONTINUED)

III - POST PLASTIC OR STABLE CRACK GROWTH

IV - BRITTLE FRACTURE OR UNSTABLE CRACK GROWTH

V - POST BRITTLE FRACTURE OR TEARING

FIGURE 4. IMPACT ENERGY REPRESENTATION

and eqn. 13 to

$$w = \int_0^t P(t)\ (dx/dt)\ dt \tag{20}$$

A third device to complement the Charpy machine is a crack detector. There are a number of common devices and methods; eg., surface applied foil and compliance techniques, but the accuracy of these is dependent on factors such as crack tip stretch and the curved nature of the crack front. Also, these only measure the one dimensional variable, a, (crack length). A device that would measure the free surface area being created as energy is being absorbed would be desirable because using

$$dA = Bda \tag{21}$$

where A = area and combining eqns. 13 and 15 to get

$$G_d = dU_e/da = dw/(Bda) \tag{22}$$

Eqns. 21 and 22 can be used to show that

$$G_d = dw/dA \tag{23}$$

Thus, immediately upon unstable crack extension G_d can be calculated and K_d values generated from eqn. 12 which can be written as

$$K_d = \sqrt{EG_d} \tag{24}$$

Furthermore, dynamic resistance to crack propagation could be determined by applying eqn. 23 after initiation.

In order to calculate fracture toughness from CVN tests, independent measurements of load, displacement and crack area during impact should be made. To date, research has centered on the production and interpretation of load-time data through the addition of strain gauges to either the tup or the anvils of the impact machine. Although results were produced, noise and discontinuities in the signal (Lum and Curll 1977) often lowered accuracy so far below that achieved in static tests that it was judged unacceptable.

One alternative to using a strain-gauge bridge was to use an accelerometer as the load transducer. Since the accelerometer uses a completely different method of determining force, it could be used in comparison to confirm or refute basic characteristics of the force-time curve.

The measurement of displacement during impact has received less attention than load determination, but is not of lesser importance since energy is the product of both. Although Barnes (1976) argues against correlating an instrumented impact energy to pendulum energy, that method is still the most logical and the easiest.

Bruch and Bowe (1977) tried a capacitive technique for measuring displacement and achieved some success. Veerling, Menken and Van Duyn

(1970) showed that there were many problems associated wih photoelectric and electrical resistance devices. With the advent of the commercially available Hall-effect transducer, it was practical to evaluate it here.

Crack-area measurement techniques were developed for quasi-static test, but two of the methods appeared capable of being used in a dynamic application. One method was to apply an insulated foil or a series-of-wires gauge to the surface of the specimen and monitor the voltage change across the gauge as the crack proceeded to reduce its conductive area. Another technique was to monitor the DC potential of the specimen itself to calculate the area of the uncracked ligament. This second method evaded problems associated wih the curved nature of the crack front and crack tip stretch and was therefore the preferable of the two.

CHAPTER II

EXPERIMENTAL PROCEDURE

PART 1 - EQUIPMENT

This chapter is devoted to the equipment used in determining the feasiblity of using an accelerometer as opposed to electrical resistance strain gauges in measuring the load on the pendulum during impact.

The Charpy machine employed a "C" type impact hammer and although reference is made (Lum and Curll 1977) to superimposed noise signals caused by tup and hammer geometries between machines during impact tests, no further information on this specific configuation was available in the literature.

For measurement of displacement of the pendulum during impact, a commercially available Hall-effect transducer was used. The Hall-effect is the physical phenomenon of metallic materials to undergo a rise in potential over their length as they enter a magnetic field. By attaching a magnet to the frame of the CVN machine and the sensor to the pendulum, a rise in voltage could be detected as the pendulum (and sensor) neared the magnet, and a drop as it continued away.

The sensor was placed above the tup (see Fig. 5) and the magnet placed level with the sensor when the pendulum was at the bottom of its swing. Displacement was calibrated through the line of action of the centre of percussion. By having the sensor and magnet remote from the tup there was less likelihood of it being damaged during impact. Because

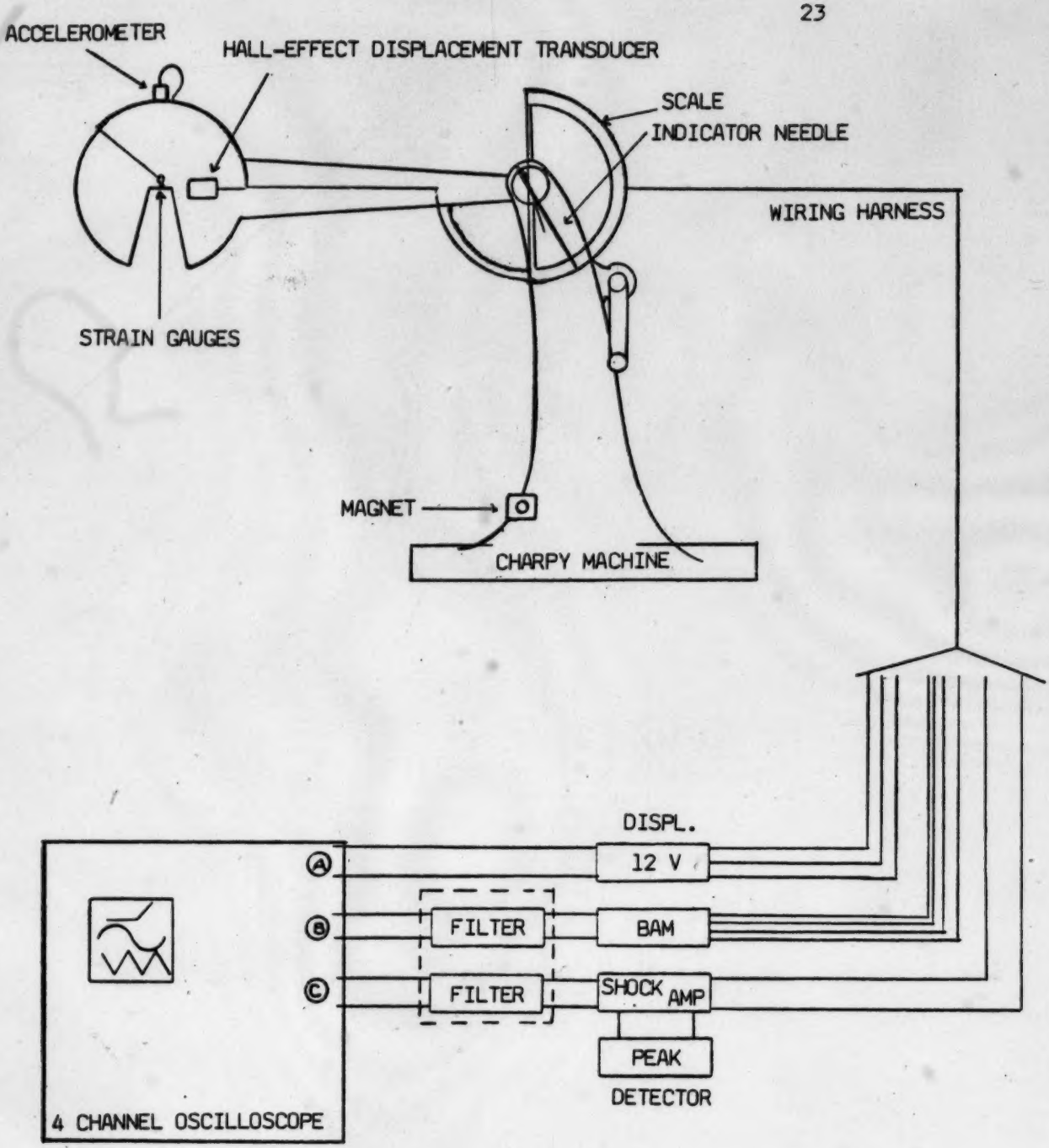

FIGURE 5. EQUIPMENT SCHEMATIC

of the two part nature of the transducer, it did not interfere with the motion of the pendulum or the test piece.

For force determination, an accelerometer was mounted on the side (of the pendulum) opposite the tup. The system was precalibrated by the manufacturer. It had a natural frequency in the range of 12,000 Hz which was excited during impact and required the use of a cut-off electronic filter. It was sensitive to lateral motion; specified by the manufacturer to be less than two percent of the total output. Because of its placement at the back of the pendulum, and because different oscilloscope channels showed small time differences in events known to be simultaneous, it had a time delay of about 0.1 msec relative to the strain gauge signal.

Another force determination was taken using strain gauges mounted in the tup. It suffered hysterisis during calibration. The time base was provided by a four channel oscilloscope. A single sweep of the beam traced displacement and the two "force" measurements. The images were then photographed. Figure 5 is a schematic of the equipment. Also, a series of static bend tests were performed using a machine that measured force and displacement of the cross-head.

Since the accelerometer required an electronic filter, and the filter introduced a time delay of 0.2 - 0.3 msec, the filter was also used on the strain gauge signal to help preserve simultaneity. The

filter introduced a reduction of two percent in the amplitude of the signals that went through it. Since the reduction was small in comparison to the overall signal, it was not deemed detrimental to the overall accuracy. Unfortunately, the filter could not be used on the displacement signal (because its upper limit was 10 volts and the Hall-effect transducer output ranged from 8 - 11 volts) and provisions had to be made (see Part 2) for matching displacement to force.

The steels from which the Charpy specimens were machined are listed in Appendix IV. They were all tested at $20^{o}C$.

PART 2 - CALIBRATION

The Hall-effect displacement transducer coupled with the magnet in a slide-by mode had a practical sensing range of 20 mm. The output was a symmetric wave with a peak of 3.3 volts. Due to the flattening at the top of the wave, it could not be calibrated easily in its mid-range between 8.9 and 11.1 mm (above 3.2 volts). The transducer was calibrated statically using an extensometer with resolution of ±0.013 mm, and the output read directly from the oscilloscope at 1.0 V/cm. Photographing the image reduced it by a factor of 0.782. In measuring the displacement from the photograph, a system of 30.8 units to the cm was used. Thus, the resolution was ±0.05 mm. The accuracy was estimated at ±2 percent since concurrent runs differed by less than that amount and the accuracy of the extensometer was approximately the same.

The output wave did not lend itself to a simple mathematical description so displacement was read directly from a calibration chart. To ensure simultaneity of events, the displacement of the pendulum at specimen contact was noted and the beginnings of the strain gauge and accelerometer trace rises were related back to that point.

The strain gauge output was calibrated statically by placing a proving ring against the back of the pendulum and applying loads through the line of action of the pendulum against a facsimile specimen. The accuracy of the proving ring was ±0.1 percent and the resolution ±8 N.

The range of calibration was 0-15200 N with a maximum transducer output of 2.5 volts. It was read at 0.5 V/cm and the final resolution was ±30 N. Accuracy was estimated at ±3 percent of reading since the furthest deviation from linear (including hysterisis effects) fell within that limit. A linear regression yielded the equation

$$P = \text{LOAD (N)} = 6060 \times \text{VOLTS} + 40 \qquad (25)$$

Lum and Curll (1977) used AISI 4340 steel specimens and calibrated an instrumented tup in a "C" type hammer. The energy calculated from the load-time data differed from the pendulum energy by less than 0.2 percent at the 21 J level. They also showed that a representative load as measured by the strain gauges differed by less than 2.5 percent from that calculated using their normalized dial (pendulum) energy calibration method. Further, the standard deviation in energy was found to be less than three percent, and in load, less than two percent.

The accelerometer system was precalibrated by the manufacturer. The range was 0-250 g with full scale output of five volts. It was monitored at 0.2 V/cm for an overall resolution of ±35 N. The accuracy stated by the manufacturer was ±5 percent in shock and the calibration is as follows

$$P = \text{LOAD (N)} = 11100 \times \text{VOLTS} \qquad (26)$$

The CVN machine had a resolution of $\pm 0.25^{o}$ leading to a maximum of ±2 percent deviation in the calculation of energy. The equation used to determine energy absorbed from eqn. 1 was

$$CVNE = \text{Energy (J)} = 154.8 \, (\cos \theta_{CVN} - \cos \theta_{Free}) \qquad (27)$$

No data on the use of accelerometers with CVN impact machines was found in the literature.

CHAPTER III

RESULTS AND DISCUSSION

PART 1 - DISPLACEMENT

The displacement-time curve during a CVN test derived from the Hall-effect transducer oscilloscope trace showed a discontinuity at the mid-point of its range where the sensor was difficult to calibrate (see Fig. 6). Although this seemed critical in determining actual displacement, it was not. The discontinuity was caused by the transducer's sensivity to lateral motion and that motion was provided by the pendulum as it impacted the specimen. (See Chapter IV, Part 4 for a discussion of the lateral motion).

From eqn. 18 it would be expected that the change in velocity of the pendulum during impact would cause the displacement to curve downwards with slope decreasing from the initial to the final velocity. Also, the rate of change of velocity as derived from the displacement should equal the acceleration of the accelerometer. In only one of the tests conducted was the acceleration constant enough (over more than 80 percent of the time) to check these relations. For Test No. 16, the velocity of the pendulum under the influence of gravity from a height of 1.08 m to nadir of swing was 4.84 m/sec. The pendulum came to a complete stop. The initial velocity from the displacement curve was calculated to be 4.66 m/sec and the length of impact time was 9.5 msec. Thus, the average deceleration required to reduce velocity to zero was 490 m/sec^2. Accelerometer results averaged 500 m/sec^2 which may be exceptional agreement.

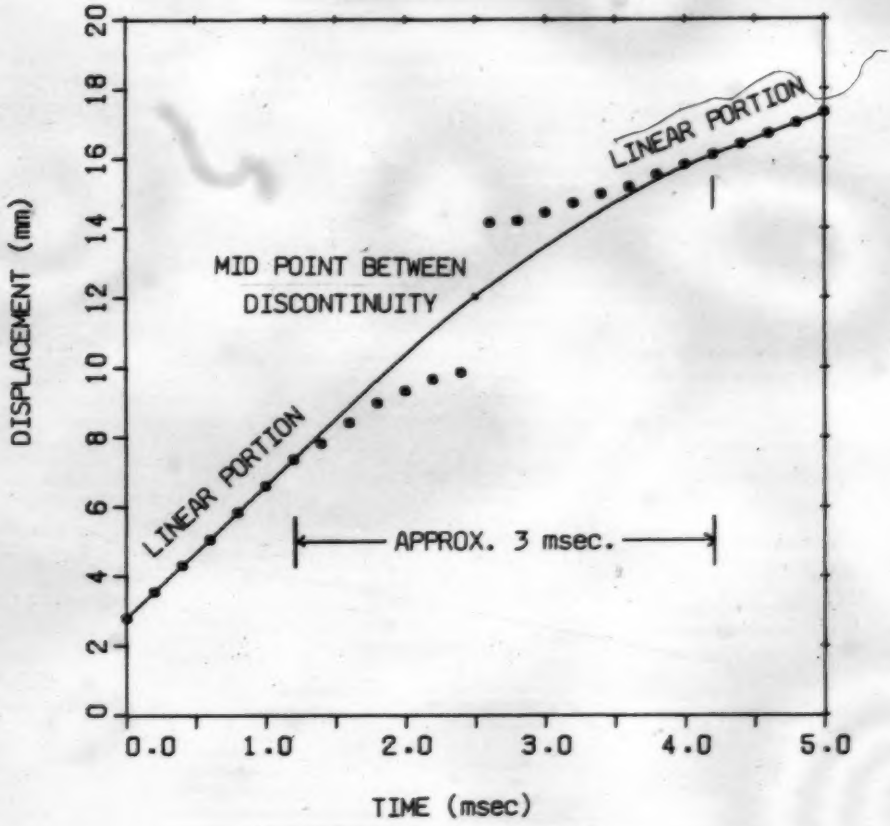

FIGURE 6. TYPICAL IMPACT DISPLACEMENT PLOT
(DISPLACEMENT AS MEASURED BY HALL-EFFECT TRANSDUCER)

From the above, it can be stated that the displacement curves were realistic at their extremities.

In order to use the complete displacement-time data, certain assumptions were made. End portions not distinguishable as curved were considered linear and the curved middle portion was assumed to bisect the discontinuity. Velocity calculations at that point differed from those derived from the accelerometer by less than five percent.

The plot of time-displacements for three tests of increasing CVNE levels (Fig. 7) showed increasing deviation from linearity as the specimen toughness increased. This was a sensible result as the impact time (time decelerating) was longer for specimens that bent before breaking. Impact times ranged from 1.3 msec at the 10 J level to 13 msec at the 160 J level. From the data, it was shown that at the 80 J level, the linear displacement approximation used in determining total energy yielded 2 J (three percent) less than when the actual displacement was used, and at the 140 J level, the difference was 33 J or 25 percent. This occurred because the load was always greatest during the early time of impact and for the tougher steels, displacement was greater during the same period. As a result of this, energy calculations were not based on linear displacement assumptions above the 40 J CVNE level.

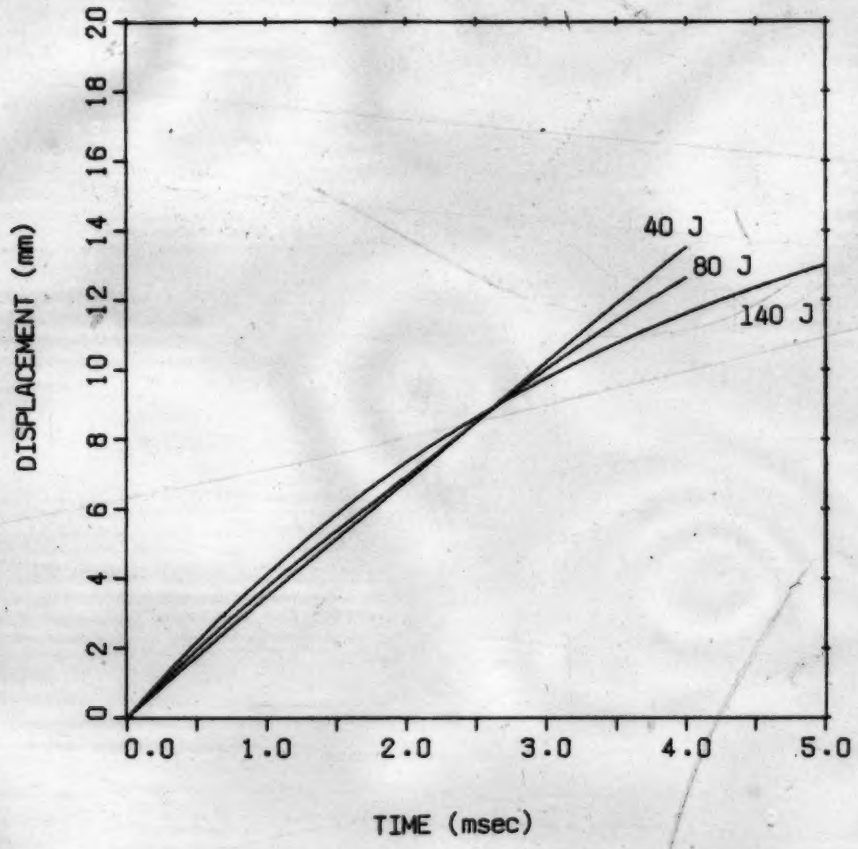

FIGURE 7. DISPLACEMENT CURVES FOR INCREASING ENERGY LEVELS
(ENERGY AS MEASURED BY PENDULUM HEIGHT
DISPLACEMENT AS MEASURED BY HALL-EFFECT TRANSDUCER)

Mathematically, this can be stated as the increased accuracy of using eqn. 20

$$W(t) = \int_0^t P(t)\ (dx/dt)\ dt$$

over

$$W(t) = (V_{av}t)\int_0^t P(t)\ dt$$

above the 40 J level of CVNE.

PART 2 - FORCE: BY STRAIN GAUGES AND BY ACCELEROMETER

Dynamic load signals in the CVN test had a superimposed characteristic ringing identified by Fisher and Hills (1982) to occur at 1600 Hz. In this set of tests, it occurred at a frequency closer to 900 Hz as identified from both the strain gauge and accelerometer signals (see Appendix V). Since it had already been decided to use an electronic filter (Chapter II, Part 1), it was set to cut off at 3000 Hz for both the strain gauge and accelerometer signals. This cut-off level filtered the natural frequency noise of the accelerometer without detracting from ringing which was considered a valid test signal.

For specimens absorbing more than 80 J, a perturbation, herein called a quasi-yield point, was discernible on the oscilloscope trace (see Appendix V). It cannot be termed yield because static three point bend tests of the same materials did not show the same drop in load, and in all cases except for 50 T plate and TTE STE 26, the static yield could be found only by applying the 0.2 percent offset criterion. This perturbation in the load-time representation could have been what is commonly termed "pop-in". The high strain rate of the test would account for pop-in in that it produced a state of strain similar to that encountered in larger test pieces at low rates of testing (such as occurs in K_{Ic} tests) where pop-in is known to occur.

In comparison to the strain gauge curve, the accelerometer showed a slower rise time (by factors ranging from one to four), a longer total

impact time (by factors ranging from 1 to 1.3, average of 1.12), lower values of maximum load below the 40 J level (by as much as 50 percent) and detected no quasi-yield point. Since the accelerometer was sensitive to lateral acceleration, a signal could be distorted by a twisting of the pendulum. Another explanation could be that the accelerometer was slow to respond and slow to decay.

PART 3 - COMPARISONS TO STATIC TESTS

In order to assess which force representation, that of the strain gauges or of the accelerometer, was more realistic, characteristics of the dynamic tests were compared to those of static three point bend tests for each of the types of steel used.

An equation to determine stress in static three point bending for a notched specimen was given by Kotilainen and Sirkkola (1981) as

$$\sigma = P/(C_f B(W-a)^2)$$

and using the constraint factor $C_f = 1.21$ (Server, Ireland and Wullart, 1974) the equation for a Charpy specimen reduces to

$$\sigma = 5.165 \times 10^{-2} P \qquad (28)$$

where stress is in MPa and Load (P) in N. Using the yield point suggested by Clausing (1970), where yield occurs at 0.025 mm plastic displacement, the yield stresses can be calculated.

For dynamic considerations P was derived using eqns. 25 and 26. Yield was taken as the quasi-yield point (when it occurred). For ultimate strength (modulus of rupture) eqn. 28 was applied despite the fact that the quantities (W-a) and C_f could have been altered by plastic deformation.

Determinations of slope (MN/m) were also made for the three force-time curves. In the case of the strain gauge output, the slope was very difficult to measure from the photographs and accuracy may have been only ±20 percent. Table II shows the resulting comparison.

There were several trends noticible from stress comparisons. With the exception of CHT 100 which broke at a stress lower than static yield, the yield stress as determined from strain gauges was always higher than the static bend yield stress. This was consistent with what is known of dynamic yield and the findings of Kotilainen and Sirkkola (1981). The ultimate strength (US) found by strain gauges was also (with the exception of CHT 100) higher than that of the static bend test. No conclusions could be drawn from this because the method used for determining US was derived for elastic strains. Comparisons of the slope of the force-displacement curves showed a correlation of 89 percent despite inaccuracies in the dynamic strain gauge slope determinations. The magnitude of the slope averaged only 86 percent of its static counterpart.

The ultimate stresses as measured from the accelerometer showed agreement with those of the strain gauges above the 80 J level (Test No. 6, Table III). Below that, it underestimated them by an approximate factor of 0.5. The slope of the force-displacement curve during elastic deformation as calculated by the accelerometer was lower than that of the static bend by factors of two to five throughout. The correlation between the accelerometer slope and the static bend slope was 31 percent. Thus, it did not faithfully reproduce known qualities of the steel as found by static tests.

TABLE II

COMPARISON OF STATIC AND

DYNAMIC LOAD DISPLACEMENT CURVES

TYPE	TEST	YIELD (MPa)		ULTIMATE (MPa)			SLOPE (mN/m)		
		STATIC BEND	STRAIN GAUGES	STATIC BEND	STRAIN GAUGES	ACCEL.	STATIC BEND	STRAIN GAUGES	ACCEL.
CHTI00	1	1125		1255	850	335	36.2	37	8.0
4340	2	705		945	1120	595	32.0	31	6.0
A516	3	320		400	610	325	27.6	14	6.5
4140	4	665		855	1010	665	36.8	29	10.0
4140	5	665		855	1030	670	36.8	30	8.0
A516	6	320		402	695	625	27.6	18	6.5
A516	7	320		402	705	610	27.6	17	6.0
50T	8	275	635	550	730	695	20.0	19	7.5
50T	9	275	630	550	705	705	20.0	18	4.5
8620	10	435	740	690	830	820	16.1	14	7.5
50T	11	275	630	550	735	700	20.0	17	6.5
50A	12	505	695	645	835	910	18.9	18	5.5
8620	13	435	795	690	895	875	16.1	19	7.0
50A	14	505	720	640	850	945	18.9	17	7.5
50A	15	505	745	640	875	840	18.9	17	7.5
TT Ste26	16	335	635	620	785	800	21.0	26	9.5

CHAPTER IV

ENERGY CONSIDERATIONS

PART 1 - RECAPITULATION

The equations for calculating fracture toughness parameters from Charpy impact tests are known. In particular, eqn. 17 can be applied to any portion of the CVNE required under the definition of the parameters eg., elastic or initiation energy. It remains to provide equipment that will measure the required variables to an acceptable degree of accuracy at any point in time to allow computation of the desired toughness parameters.

Two tests of accuracy were applied. First was the comparison of dynamic results to static results to see if the load-displacement curve conformed to a sensible configuration. In Chapter III it was shown that the strain gauge results were realistic, while the accelerometer results consistantly deviated in the elastic region and even in the plastic region when the specimen absorbed more than 80 J. The second test was to compare total energy calculations of the instrumentation against the CVN machine pendulum energy. If individual points on the load-displacement curve were acceptable and the total energy was correct, portions of the total energy up to the individual points could be considered correct.

PART 2 - ENERGY CALCULATIONS

Using the displacement curves of Chapter III, the energy calculations were made using the averages over the periods of rising, level, declining and tailing force. Account was taken of the various time delays (Chapter II, Part 1 and Chapter III, Part 2) so that measurements were simultaneous. On occasion, the tail portion of the force trace ran off the graph, so linear extrapolations to the baseline were used. The energies so calculated are listed in columns II and III of Table III. Column I shows the CVNE obtained from eqn. 27.

A statistical analysis on the results produced a correlation of greater than 99 percent between both of the instrumented energies compared to the pendulum energy. Both had average errors of 8 percent, but the largest error was 23 percent at 26 J for the strain gauges and 16 percent at 101 J for the accelerometer.

Although the results from the accelerometer were comparable to those of the strain gauges, they added no new information to the test. Also, because of the slower rise time of the load signal, they tended to detract from elastic fracture toughness considerations.

The strain gauge bridge appeared acceptable under both tests and (for this application) was the preferrable of the two.

TABLE III

CVNE BY VARIOUS METHODOLOGY

TEST #	SPECIMEN TYPE	I CVNE PENDULUM J ± 2%	II CVNE STRAIN GAUGES J ± 5%	III CVNE ACCELEROMETER J ± 7%
1	CHT 100	18	16	17
2	ASTM A516 GR70	26	32	30
3	AISI 4340	31	29	28
4	AISI 4140	39	37	35
5	AISI 4140	43	39	40
6	ASTM A516 GR70	80	70	77
7	ASTM A516 GR70	80	71	70
8	50T	101*	116	117
9	50T	104*	108	117
10	AISI 8620	133*	127	137
11	50T	143*	146	144
12	50A	150*	144	160
13	AISI 8620	151*	141	134
14	50A	162*	158	178
15	50A	162*	161	154
16	TT Ste 26	268*	260	283

* Specimen did not break.

PART 3 - K_{Ic} AND K_{Id} FROM CVNE

Fracture toughness values were generated using prominent correlations in the literature as shown in Appendix II. For the steels tested, averages of impact energies (CVNE) and load at fracture (P_f) for four or five specimens were used in the equations (see Table IV). Published values or extrapolated values from the text of Barsom and Rolfe (1970) are included where possible.

Below the 80 J level, P_f as determined from the accelerometer was approximately one-half of the P_f determined from the strain gauges. This is consistent with the measurements of UTS made as in Table II. Closer inspection revealed that for both cases, as CVNE approached 80 J, the load (and therefore stress) determined by the accelerometer progressively approached the magnitude of the load as determined by the strain gauges. The discrepancy below the 80 J level was therefore caused by a slower response of the accelerometer. Proof that this discrepancy was not caused by a calibration error occurred in the case of ASTM A516. During the testing it was found that half the specimens broke at the 27 J level and half at the 80 J level. Those breaking at 27 J had an accelerometer response indicating only 50 percent as high a load as the strain gauges indicated, while at the 80 J level the calculated loads were the same.

TABLE IV

K_{Ic} FROM CVN DATA

I $K_{Id} = 0.002\ P_f$ (SG)

II $K_{Id} = 0.002\ P_f$ (ACC)

III $K_{Id}/E = 0.64 \times 10^{-3}$ (CVNE)

IV $K_{Id} = 15.5\ (CVNE)^{0.375}$

V $K_{Ic}/E = 0.22\ xz\ 10^{-3}\ (CVNE)^{1.5}$

VI $K_{Ic} = 19\ (CVNE)^{0.5}$

				I SG	II ACC	III	IV	V	VI	PUBLISHED	
MAT'L	CVNE J	$P_{f(SG)}$ kN	$P_{f(ACC)}$ kN	K_{Id} MPa $\sqrt{m}$	K_{Id} MPa $\sqrt{m}$	K_{Id} MPa $\sqrt{m}$	K_{Id} MPa $\sqrt{m}$	K_{Ic} MPa $\sqrt{m}$	K_{Ic} MPa $\sqrt{m}$	K_{Ic} MPa $\sqrt{m}$	K_{Id} MPa $\sqrt{m}$
CHT 100	18.0	16.5!	6.9!	34	14	48*	46	58	80		
A516	27	11.8!	6.2!	24	13	59	53	79	99	150 o	
4340	30.0	21.6!	11.5!	44	24	64*	56	86	104	103	
4140	39	18.6	12.4!	38	25	72*	61*	105	118*	95	
A516	80	11.8!	11.9!	24	24	102	80	179	169	150 o	
50T	100	12.9	12.6	26	26	114*	87	212*	190*	120 o	60-100
8620	143	13.6	12.9	27*	26*	137*	99*	277*	277*		
50A	158	15.5	15.8	32*	32*	144*	103*	299*	238*		

! P_f Max. Load

* Exceeds one or more limits placed on formula

o K_Q

The results in Table IV were reproduced in Fig. 8. Curves I and II of Fig. 8 show K_{Id} as determined by correlation to P_f. Despite the differences seen between K_{Id} values below 80 J as determined by strain gauge and accelerometer load measurements, the general trend was for the derived K_{Id} to be relatively constant over the range of energy levels tested. This was a direct consequence of the fracture load remaining relatively stable over that range. In comparison, curves II and III, which were from K_{Id} - CVNE correlations, show an increase in K_{Id} as CVNE increases. In the case of 50 T steel where a comparable K_{Id} value was published (see Table IV) it agreed closely with the results of the K_{Id}-CVNE correlation while the K_{Id} - P_f correlation underestimated it by a factor of three to four. Although the P_f formula was developed for medium to low strength steels (NMAB 1976), Fig. 8 shows it to agree with other formulae in the region of low CVNE (typically high strength) steels. Since curves III and IV agree to within four percent of themselves in that range (and to within 30 percent overall) the previous comparison was a fair one to make. Curves V and VI were generated using K_{Ic}-CVNE correlations. They agree to within 20 percent of themselves. They are consistantly above the K_{Id} determinations as would be expected (Barsom and Rolfe 1970). No comment can be made as to the accuracy of any of the above curves since direct determination of fracture toughness was not carried out for the steels tested.

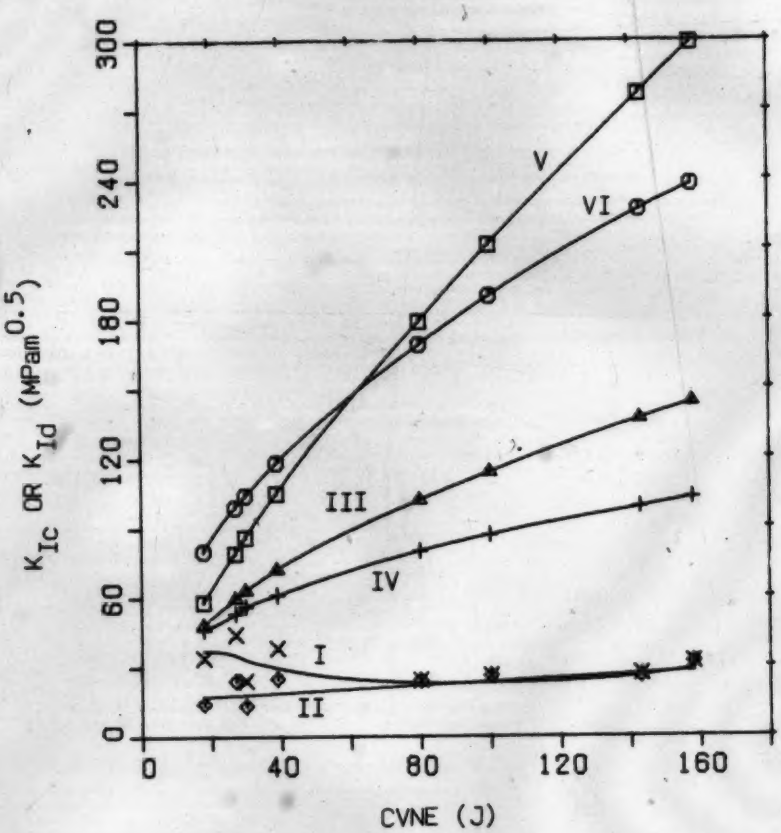

I $K_{Id} = 0.002\ P_f$ (S.G.)

II $K_{Id} = 0.002\ P_f$ (ACC.)

III $K_{Id}^2/E = 0.64 \times 10^{-3} CVNE$

IV $K_{Id} = 15.5\ CVNE^{0.375}$

V $K_{Ic}^2/E = 0.22 \times 10^{-3} CVNE^{1.5}$

VI $K_{Ic} = 19 CVNE^{0.5}$

FIGURE 8. K_{Ic} AND K_{Id} FROM CVN DATA

PART 4 - THE TWISTING, LATERAL MOTION OF THE PENDULUM

Fisher and Hills (1981) noted that during some severe impacts, if the specimen was not located precisely at the centre of percussion, an apparent backward motion of the pendulum was recorded. They attributed this to an impulse wave being sent up the suspension arm. Later, without specific reference to the above, they noted that there was an anomoluous bending action in the pendulum arm and that the energy absorbed by the specimen was 10 - 15 percent lower than that lost by the pendulum which reflected the energy losses in the pendulum arm itself.

Although the apparatus used was different, the results obtained from the strain gauges during the 16 tests showed that above the 150 J level a similar strain gauge under-estimation of energy absorbed occurred, although the difference was only one to six percent. Such a trend was not obvious from the accelerometer results.

If indeed some impact wave was caused in the pendulum, its reflections from the support should have occurred at a frequency of 3600 Hz (using the speed of sound in steel as approximately 5×10^6 mm/sec and a distance of 700 mm (x2) as the length of the pendulum for these tests). If the impact wave was considered to reflect across the 200mm breadth of the "C" of the pendulum, then ringing would have occurred at approximately 12,000 Hz (and would have been filtered out). In fact, ringing was noticed, but it occurred at 900 Hz.

If a simple lateral translation of the pendulum was assumed, it explained the discontinuity of the displacement curve and the fact that the dynamic impact output of the Hall-effect transducer never reached its maximum value as determined by static conditions. If a twisting motion was assumed, the same effect would apply.

In a simple experiment, lateral vibration was measured by impacting the pendulum dead centre on one side. The frequency was found to be five to six Hz. The twisting frequency was found to be 10 Hz. The time taken by the displacement output to break away and then rejoin its smooth-curve-path (see Fig. 6) was approxiately three msec. This one-half wave corresponded to a "frequency" of 170 Hz. It is quite possible that translational or twisting motion did occur and that the rejoining of the displacement curve was caused by the relative amount of amonolous motion becoming less significant to the total as the pendulum moved forward.

It was also noted during calibration that if the pendulum was allowed to twist, strain gauge load readings were below expected values. This could account for the dynamic loss of one-to-six percent in tough specimens when the most twisting would have occurred.

Finally, some lateral or twisting motion was known to occur because in tests where the pendulum came to a complete stop or was severely retarded, the lateral space between the Hall-effect transducer and the magnet (approx. three mm) was insufficient to prevent contact between them, causing them to be broken.

CHAPTER V

D.C. POTENTIAL CRACK DETECTOR

PART 1 INTRODUCTION

It has been shown (eqns. 21 and 23) that measurements of energy absorbed per unit area created by the initiation and propagation of a crack in an impacted test piece would allow direct computation of G_d and other fracture toughness parameters for a material. Chapters II, III and IV dealt with the physical measurement of energy absorbed and in particular, the ability to measure predefined portions of the total energy of fracture. A D.C. potential method of directly monitoring the area of the uncracked ligament in front of the crack tip would provide the only other measurement required for G_d determination.

An attempt was made to detect crack initiation and measure crack propagation during a Charpy V-Notch (CVN) impact test using a D.C. potential difference method. Two types of constant current supplies, two methods of wiring, four types of probe contacts, electronic filtering and mechanical stabilizing elements were used in an effort to gain accurate and reproducable results.

PART 2 THEORY

Using a power supply to provide a constant current through the specimen, the voltage across the specimen can be monitored and should show a rise as the advancing crack decreases the conductive area. From Halliday and Beevers (1980) the steady electrical potential Φ at a point (x, y) for a homogeneous specimen with current flow perpendicular to the crack plane is given by:

$$\partial^2\Phi/\partial x^2 + \partial^2\Phi/\partial y^2 = 0$$

Given that the current is uniform (current leads are far from the crack plane), and the influence of notch is ignored, for a specimen configuration is as in Fig. 8, the potential difference between point P and the crack plane is given by:

$$V = IM(K_a \cos^{-1}\Psi) \qquad (29)$$

$$\Psi = \cos(Z/2W)/\cos(a/2W)$$

where, Ka = proportionality constant depending on the geometry, resistivity, and current Z = f + i x, and W,a = as in Fig. 9.

From this analysis, it was shown that placing the leads of the sensor at increasing distances from the V-notch had the effect of increasing reproducibility while decreasing sensitivity.

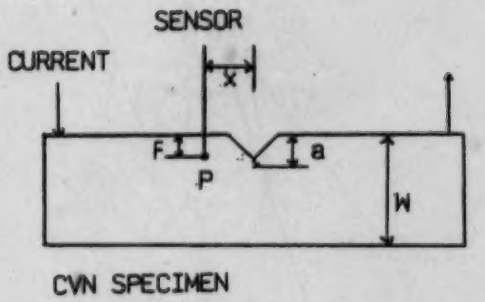

FIGURE 9. VARIABLES FOR THEORETICAL CALIBRATION

It was decided to use a direct method of calibration (comparing actual cracked surface increases to actual voltage increases) rather than a theoretical method, thereby bypassing errors due to the assumptions of eqn. 29 and the accuracy errors inherent in the measuring instruments. Also, it was decided to place the sensor probes far from the crack plane (see Figs. 9 and 11) as would best suit this method of calibration. The sensitivity was approximately 0.25 percent voltage change per percent area reduction, whereas Knott (1980) achieved three times that sensitivity by placing the sensor leads near the "V".

PART 3 EXPERIMENTAL

A Hewlett-Packard Model 6286A constant current supply was used to provide 10 amps through the specimen. The power demand was of the order of 0.02 watts. However, with the low (2mV) voltage across the specimen, 60 cycle noise generated internally by the supply made this apparatus unsuitable and it was used only to determine the resistance of specimens in a static condition and for static calibration.

A 12 volt automobile battery and one ohm resistance (see Fig. 10) was used to supply a constant current for dynamic testing. Since the resistance changed as the resistors heated up two methods were tried to cool them. First, a refrigeration unit was employed to pump glycol at $0^{o}C$ through a plastic tube wrapped around a one ohm resistor. Second, four one ohm resistors were connected - two in parallel in series with another two in parallel - and cooled with a fan. Both systems worked so the simplest (second) was chosen. This system produced approximately 10.7 amps.

A type S46B Tektronix oscilloscope with an output of 0.9 V/Div for input of 0.2 mV/Div was used to amplify the signal by a factor of 4500.

The rest of the commercially available equipment was as described in Appendix III. The four-channel oscilloscope introduced a gain of five to the output of the first oscilloscope for total signal amplification of 22500. The filter introduced a time delay of 0.2 - 0.3

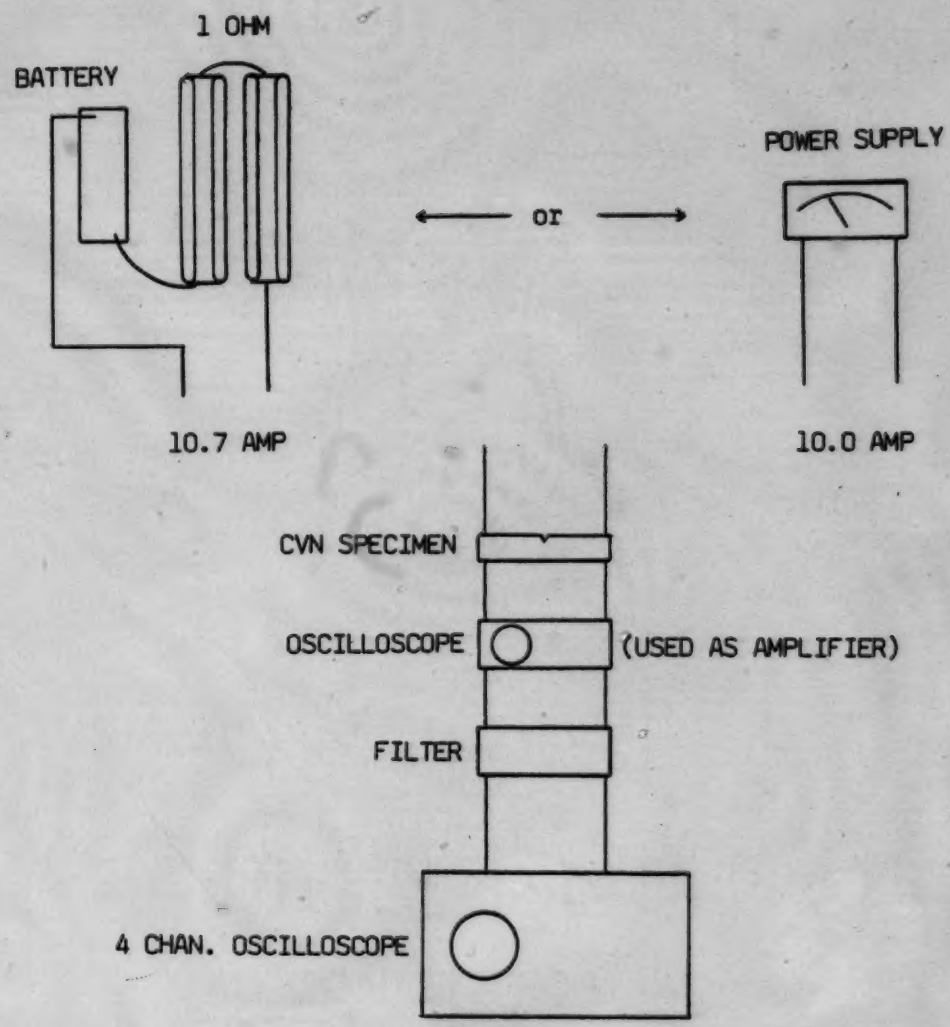

FIGURE 10. CRACK DETECTOR EQUIPMENT SCHEMATIC

msec and reduced the amplitude of a comparable signal by two percent when the cut off was set at 3000 Hz. New anvils were made for the CVN machine so that a layer of dielectric tape could be placed between a set of inserts that held the specimen in place.

Four types of probe contacts were tried. Single lead contacts (see Fig. 11) were used initially but discarded when it was found difficult to reproduce the contact (soldered) resistance where the wires met. They produced a total initial resistance of 0.28 - 0.4 mohm which was 0.1 - 0.22 mohm above the specimen resistance due to contact resistance at the specimen. Surface soldered single lead contacts (see Fig. 11) produced essentially the same results. Internal soldered single lead contacts (see Fig. 11) had an initial resistance indistingnishable from specimen resistance, but were difficult to produce and handle. They were used for dynamic testing.

Double lead contacts (See Fig. 11), although they produced initial total resistance of 0.18 - 0.24 mohm, were used for reasons of simplicity in generating the calibration curve.

Two wiring harnesses were tried. Single conductor wires throughout and shielded single conductor wires. It was found that shielding the current-carrying and probe wires had a small beneficial effect on the signal. They were difficult to work with because of their stiffness and often required that the specimen be taped onto the anvils to prevent movement before pendulum contact. They were used despite this drawback.

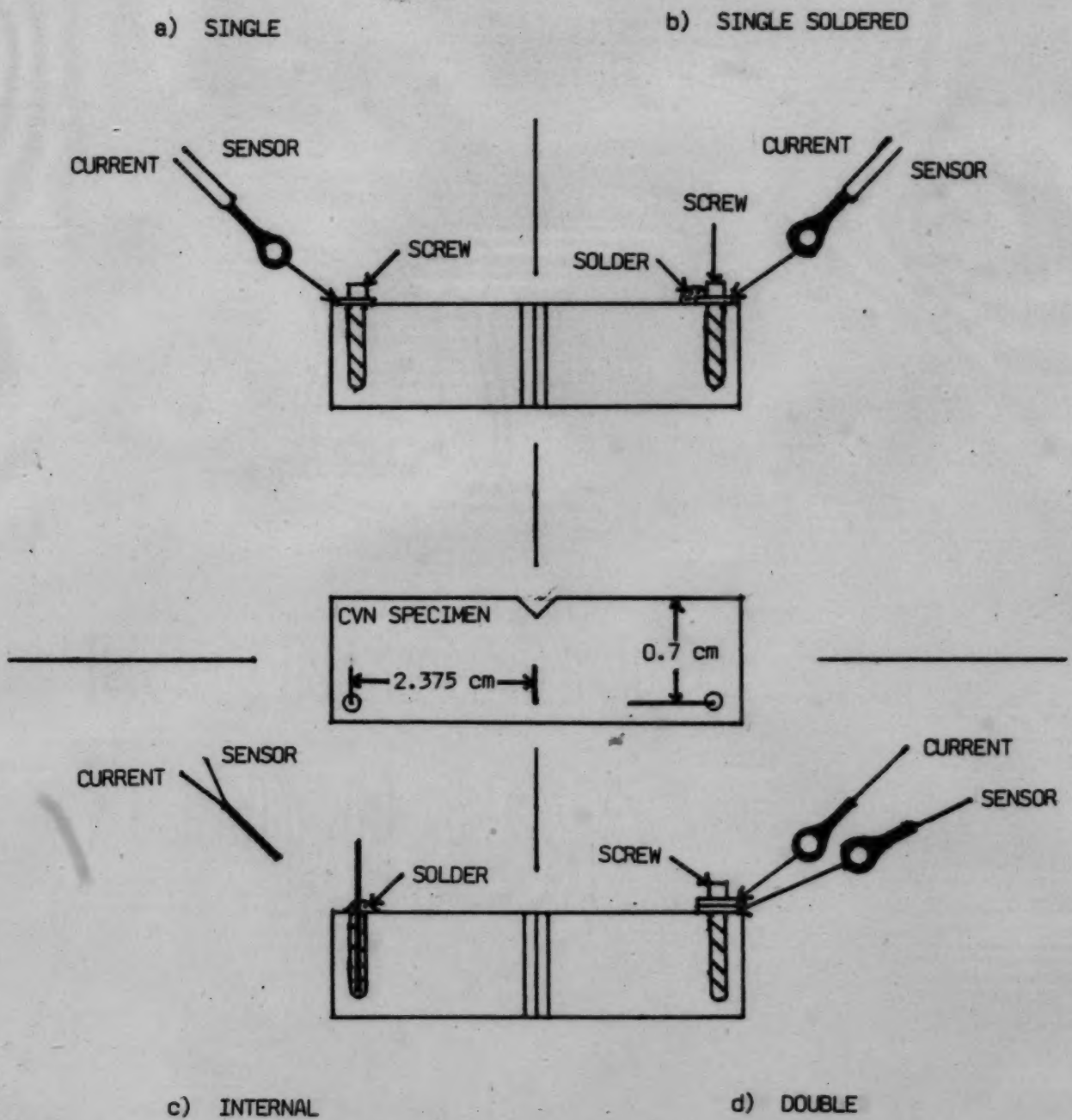

FIGURE 11. POWER AND SENSOR LEAD CONNECTIONS

PART 4 CALIBRATION

To test the system's ability to detect changes in cross sectional area, eight strands of 16-gauge wire were connected in parallel and substituted for the specimen. Changes in potential were recorded as the wires were cut one by one.

The system with a Charpy specimen was calibrated quasi-statically in the following manner. The apparatus was assembled with the power supply as in Fig. 10. The time base on the oscilloscope was set to an extremely fast rate to focus on a flat portion of the output and initial values of voltage were recorded. The pendulum was allowed to impact the specimens from increasing heights and the rise in voltage from a visible crack was noted. The crack itself was painted for later measurement. Voltage decreased to 80%-50% of its original value as the specimen temperature dropped (after being heated by the impact). This precluded using a specimen for more than one crack area correlation. The procedure was repeated for nine specimens of ASTM A516 grade 70 steel.

In trying to obtain a dynamic record of percent area vs time during an impact test, the battery and one ohm resistance network were substituted for the power supply. The pendulum was allowed to fall through 94.6^{o} producing 167 J of energy on impact. The Hall-effect transducer and magnet were used to give a calibrated record of pendulum displacement and also to trigger the scope approximately 1.5 mm from pendulum contact. The filter was set to 3000 Hz cut-off so as to duplicate the load results of Chapter IV.

PART 5 RESULTS

The eight-wire experiment, although a poor analogue of specimen cracking, was itself quite accuracte. Excepting one wild point, calculated average resistance of remaining wires per cut had a standard deviation of five percent (inclusion of the wild point increased this to eight percent). Fig. 12 shows the results.

The quasi-static calibration of CVN specimens was not so accurate. The results are presented in Fig. 13. A linear regression was performed on the data with a correlation of 94 percent. Calculated resistance of remaining areas had a standard deviation of 12 percent.

The dynamic results were not representative of the voltage change as the crack ran across the specimen. Fig. 14 shows the typical results from an impact test. The voltage rise occurred in two stages. First was a slow rise before impact and second was a sharp increase at impact. The sharp rise occurred identically to itself every time (within limits of measurement) and was independent of load or specimen-type.

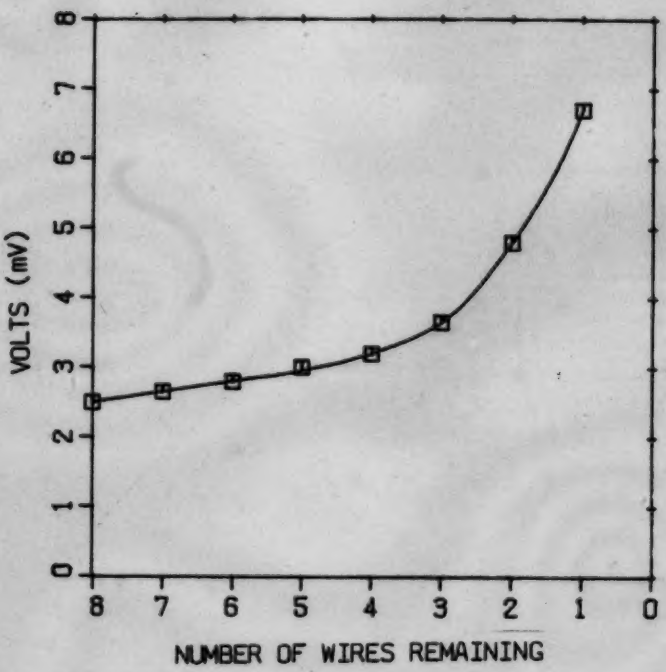

FIGURE 12. EIGHT WIRE ANALOGUE

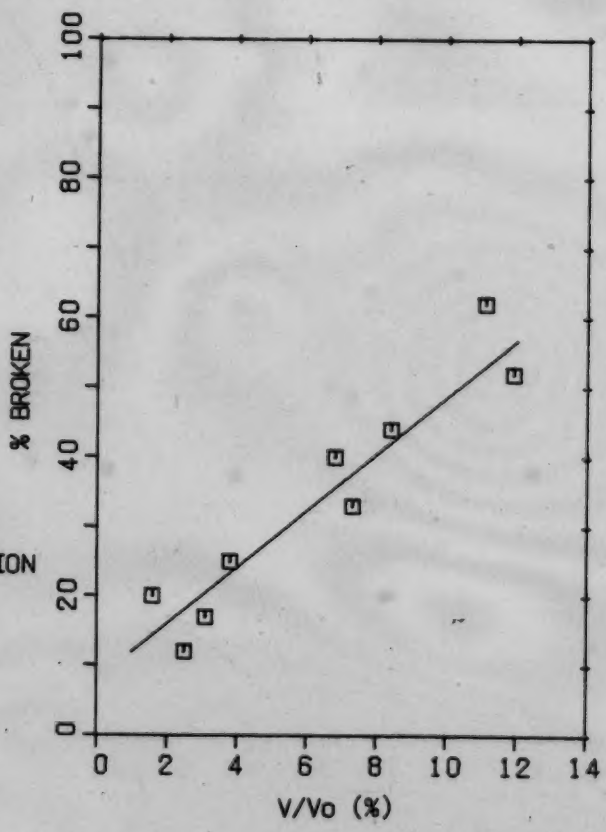

FIGURE 13.
CHARPY QUASI-STATIC CRACK CALIBRATION

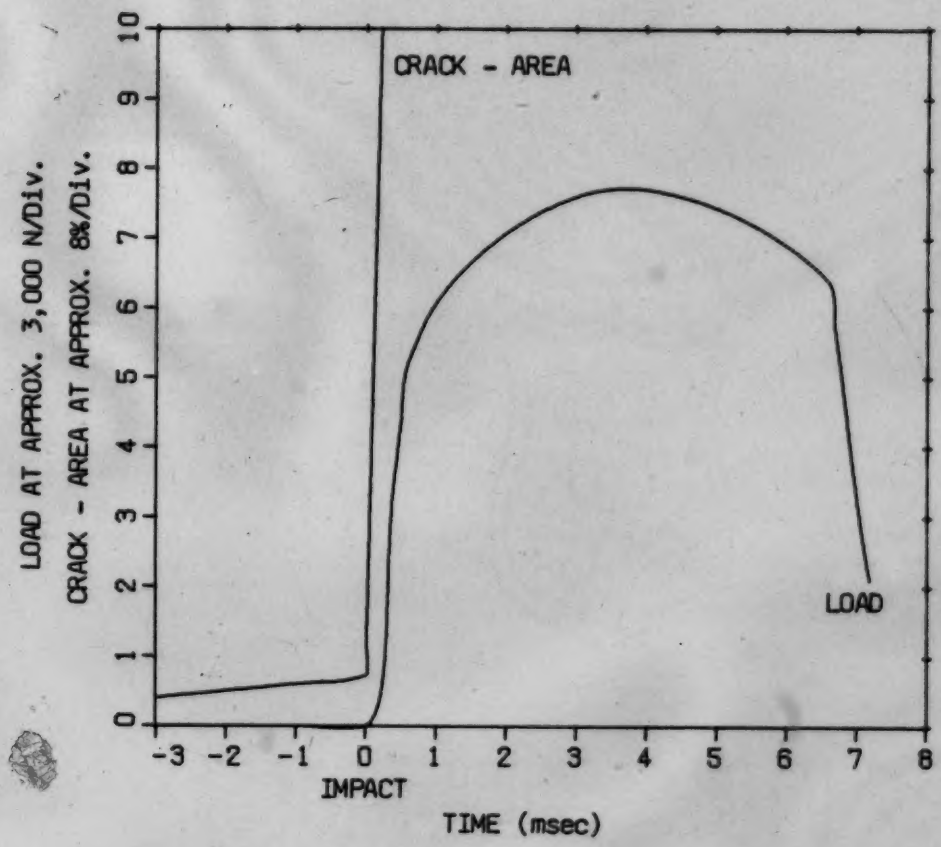

FIGURE 14. CRACK - AREA AND LOAD REPRESENTATION OF RESULTS FOR CVN IMPACT TESTS

PART 6 OBSERVATIONS

The quasi-static calibration chart (Fig. 13) is a linear regression of a relation known by eqn. 29 to be non-linear. However, Knott (1980) showed that for a single edge notched specimen, theoretical and experimental values are approximately linear above 10 percent broken (above $a/a_0 = 1.3$ in his notation). Also, the correlation coefficient for the calibration chart was 94 percent making it acceptable for experimental purposes, but insensitive to small deviations from linearity.

The dynamic response was affected by two influences other than the reduction of conducting area in the specimen. The first was a pendulum effect. As the pendulum approached the specimen, a voltage was induced in the lead wires (see Fig. 14). The magnitude of this voltage rise was reduced to its minimum of 0.02 mV by keeping the sensor wires together and shielded thus right up to the specimen. The second influence was an impact effect. Immediately upon pendulum contact, a voltage of greater than five mV was induced. The magnitude of this effect precluded monitoring voltage change due to crack propagation. The impact could not be filtered out electronically because it lasted approximately as long as the impact.

Both the pendulum effect and the impact effect occurred when a specimen was broken without the 10 amps current through it. The impact effect also occurred when striking it with a piece of wood although the

amplitude was reduced to 0.02 - 0.06 mV. Since the crack measuring system was not grounded and the pendulum was, it is possible that a capacitive effect between the pendulum and the specimen or the specimen and the anvils was responsible for the rise in voltage. This would then explain why the effect occurred without the 10 amps supplied.

Heat effects also influenced the voltage across the specimen. In obtaining the quasi-static calibration, the rise had to be measured quickly because it fell back as far as 50 percent of its initial value as the specimen cooled. This effect was dramatized by heating a specimen to approximately 50^{o}C causing an increase of more than 0.7 mV across it.

CHAPTER VI

CONCLUSIONS

1. The empirical correlations K_{Ic}-$CVNE^{0.5}$ and $K_{Ic}/E = 0.22 \times 10^{-3}(CVNE)^{1.5}$ agreed between themselves (to within 20 percent) over the range of 18-158 J CVNE. The relations $K_{Id}/E = 0.64 \times 10^{-3}(CVNE)$ and $K_{Id} = 15.5(CVNE)^{0.375}$ also agreed (to within 30 percent) in that range but gave consistantly lower values than the K_{Ic} correlatons. The relation $K_{Ic} = 0.002 P_f$ showed agreement with the K_{Id}-CVNE relatons at low levels of CVNE but remained relatively constant over the range of energies tested and therefore gave lower results than the K_{Id}-CVNE relations at high levels of CVNE.

2. A fracture toughness indicator, $K_d = \sqrt{EG_D}$, could be calculated from the results of Charpy tests provided accurate determinations could be made of load, displacement and crack area during impact.

3. The characteristic ringing or noise that occurred in the load signal at approximately 900 Hz was verified by the comparison of accelerometer to strain gauge transducer output. The accelerometer used did not provide any other useful information and although it recorded accurately the total amount of energy absorbed during impact, it underestimated know tensile properties of the more brittle steels due to its slow rise (and decay).

4. Load measurements made by the strain gauges were no more accurate than those of the accelerometer in determining total energy of impact, but were acceptable in their reproduction of known tensile properties of steels tested due to their quicker frequency response.

5. The Hall-effect transducer was found to be acceptable for monitoring dynamic displacement despite the discontinuity it produced in its mid-range. Twisting and/or lateral displacement of the pendulum was known to have occurred and was sufficient to cause such a discontinuity.

6. Assumption of linear pendulum displacement during impact produced increasing error in CVNE calculations above the 40 J level.

7. The DC potential method of measuring the area of the uncracked ligament was unsuccessful due to problems encountered in having to amplify the signal by 22,500. A capacitive effect in the system induced a voltage that was two orders of magnitude greater than a 30 percent broken signal upon start of impact. Induced voltages caused by the motion of the pendulum have been reduced to an acceptable level. Further analyses of crack propagation and DC potential method were not undertaken because of the initial results.

BIBLIOGRAPHY

AMERICAN SOCIETY OF MECHANICAL ENGINEERS (1978) Boiler and Pressure Code (8) UG-84

AMERICAN SOCIETY FOR TESTING AND MATERIALS (1982) Notched Bar Impact Testing of Metallic Materials, Ann. Book Stds. (10) Desig. E23-81

AMERICAN SOCIETY FOR TESTING AND MATERIALS (1982) Plane Strain Fracture Toughness of Metallic Materials, Ann. Book Stds. (10) Desig. E399-81

AMERICAN SOCIETY FOR TESTING AND MATERIALS (1982) Standard Terminology Relating to Fracture Testing, Ann. Book Stds. (10) Desig. E616-81

BARNES, R.C. (1976) An Evaulation of the Reliability of Instrumented Charpy Test Records, Technical Note MRL-TN-384, Dept.Def. Aust., Maribyrnong

BARSOM, J.M., ROLFE, S.T. (1970) Correlations between K_{Ic} and Charpy V-Notch Test Results in the Transition Temperature Range, ASTM STP 466 281-302

BARSOM, J.M. (1975) Development of the AASHTO Fracture Toughness Requirement for Bridge Steels, Eng. Frac. Mech., (7) 605-618

BRUCH, U., Bowe, K.H. (1977) Instrumented Impact Test with Capacitive Measuring of Displacements, Material Prufung 19(1) 21-22

CHARPY, G., GORNU-THENARD, A. (1917) New Experiments on Shock Tests and on the Determination of Resilience, Jour. Iron and Steel Inst.

CLAUSING, D.P. (1970) Effect of Plastic Strain Rate on Ductility and Toughness, Int. Jour. Frac. Mech., 6(1) 72-85

DAEVES, I.K. (1965) Werkstoff-Handbuk Stahl Und Eisen, Dusseldorf 4th Edit. (D1) 1-5

FISHER, W.F.C., HILLS, D.A. (1982) The Development of an Instrumented Impact Test Machine, Eng. Frac. Mech., 16(2) 287-294

GRIFFITH, A.A. (1920) The Phenomena of Rupture and Flaw in Solids, Trans, Roy. Soc. London, A-221

GRIFFITH, A.A. (1924) The Theory of Rupture, Proc. 1st Int'l Conf. App. Mech., Deflt

GROSS, J.H. (1970) Effect of Strength and Thickness on Notch Ductility ASTM STP 466 21-52

HALLIDAY, M.D., BEEVERS, C.J. (1980) The DC Electrical Potential Method for Crack Length Measurement, The Measurement of Crack Length During Fracture and Fatigue, EMAS 85-113

IRWIN, G.R. (1948) Fracture Dynamics, Frac. Met. ASM., Cleveland, 152-155

IRWIN, G.R. (1962) The Crack Extension Force for A Part Through Crack In A Plate, Trans. ASME Jour. App. Mech., 29(4)

KNOTT, J.F. (1980) The Use of Analogue and Mapping Techniques with Particular Reference to Detection of Short Cracks, The Measurement of Crack Length and Shape During Fracture and Fatigue, EMAS 113-135

KOTILAINEN, H., SIRKKOLA, E. (1981) The Measurement of the Cleavage Fracture Strength and the Dynamic Yield Strength by Means of an Instrumented Impact Test, Valtion Teknillinen Tutkimuskeskus Espoo (Finland)

LUM, P.T., CURLL, C.H. (1977) Variables Affecting Reproducibility of the Instrumented Impact Test, ASTM STP626 21-31

MARANDET, B., SANZ, G. (1977) Evaluation of the Toughness of Thick Medium Strength Steels by LEFM and Correlations Between K_{Ic} and CVN, ASTM STP 631 72-95

NATIONAL MATERIALS ADVISORY BOARD (1976) Rapid Inexpensive Tests for Determining Fracture Toughness, Rep NMNB-328, Nat.Ac.Sci.

OROWAN, E. (1949) Fracture Strengths of Solids, Rep. Prog. Phys., Phys. Soc. London, (12) 214

PISARSKI, H.G. (1978) A Review of Correlations Relating Charpy Energy To K_{Ic}, Weld. Inst. Res. Bull., 19(12) 362-367

PLATI, E., WILLIAMS, J.G. (1975) The Determination of the Fracture Parameters for Polymers in Impact, Poly. Eng. Sci., 15(6) 470-477

PUZAK, P.P., LANGE, E.A. (1972) Significance of Charpy V-Test Parameters as Criteria for Quenched and Tempered Steels, NRL-7483 Nav. Res. Lab., Wash.

RAWERS, J.C., McMULLEN, W.D. (1980) Fracture Energies of Zircalloy-4, Eng. Frac. Mech., (13) 979-985

RICE, J.R. (1968) A Path Independent Integral and Approximate Analysis of Strain Concentration by Notches and Cracks, Jour. App. Mech., Trans. ASME (35) 379

RITCHIE, R.O. (1978) On the Relationship Between Fracture Toughness and Charpy V-Notch Energy in Ultrahigh Strength Steel, What Does the Charpy Test Really Tell Us?, ASM Metals Park Ohio 44073, 54-73

ROLFE, S.T., NOVAK, S.T. (1970) Slow Bend K_{Ic} Testing of Medium Strength High Toughness Steels, ASTM STP 463 124-159

ROLFE, S.T., BARSON, J.M. (1977) Fracture and Fatigue Control in Structures, Prentice Hall, N.J. 92-139

ROLFE, W. (1981) Mechanical Characteristics as Determined by DIN Standards and ASTM Specifications compared, Schweissen und Schneiden 33 (12) E227-228

SAILORS, R.H., CORTEN, H.T. (1972) Relationship Between Material Fracture Toughness Using Fracture Mechanics and Transition Temperature Tests, ASTM STP 514 164-191

SERVER, W.L., IRELAND, D.R., WULLART, R.A. (1974) Strength and Toughness Evaluations From an Instrumented Impact Test. DYNATUP TR 74-29 R, Effects Tech. Calif. 1-51

SMITH, E., PATCHETT, B.M. (1975) Effects on Notch Acuity and Side Grooving on Fracture Toughness Part 1, Weld. Res. Supp. Weld. Jour., 169s-177s

VEERLING, C., MENKEN, C., VANDUYN, J. (1970) Measurement of the Load-Deflection Diagram in the Charpy Impact Test, ISI Pub.D20, Frac.Tough. H.STR.Mat'l.

WESTERGAARD, H.M. (1939) Bearing Pressures and Cracks, Trans. ASME, Jour. App. Mech., 49

APPENDIX I
DEFINITIONS

$G - [FL^{-1}]$ Crack Extension Force

The elastic energy per unit of new separation area that is made available at the front of an ideal crack in an elastic solid during a virtual increment of forward crack extension.

$J - [FL^{-1}]$ The J-Integral

A mathematical expression, a line or surface integral that encloses the crack front from one crack surface to the other, used to characterize the local stress strain field around the crack front.

$K - [FL^{-3/2}]$ Stress Intensity Factor

The magnitude of the ideal crack tip stress field (a stress field singularity) for a particular mode in a homogeneous linear-elastic body.

$K_{Ic} - [FL^{-3/2}]$ Plane Strain Fracture Toughness

The crack extension resistance under conditions of crack tip plane strain.

NOTE: - In Mode I, for slow rates of loading and negligible plastic zone adjustment, plane strain fracture toughness is the value of the stress intensity factor $[FL^{-3/2}]$ as measured under the requirement of E399.

$K_c - [FL^{-3/2}]$ Plane Stress Fracture Toughness

Crack extension resistance under conditions that do not approach crack tip plane strain to a degree required by an empirical relation. The value of K critical to crack propagation.

$K_d - [FL^{-3/2}]$ Plane stress fracture toughness under dynamic loading (impact) conditions.

APPENDIX II

(Pisarski 1978)

FRACTURE TOUGHNESS EQUATION	AUTHOR	APPLICATION
$K_{Ic} = 19\ (CVNE)^{1/2}$	Marandet and Sanz (1977)	303 < Yield < 820 crystallinity > 80%.
$K_{Ic}^2/E = 0.22 \times 10^{-3}(CVNE)^{1.5}$	Barsom and Rolfe (1970)	270 < Yield < 1700 Structural steels transition temp. region
$(K_{Ic}/\sigma_y)^2 = 0.64\ (CVNE/\sigma_y - 0.01)$	Rolfe and Novak (1970)	760 < Yield < 1700 Upper shelf transition curve at 27°C.
$K_{Id}^2/E = 0.64 \times 10^{-3} CVNE$	Barsom (1975)	250 < Yield < 345 Transition temp. region
$K_{Ic} = 14.6\ (CVNE)^{0.5}$	Sailors and Corten (1972)	410 < Yield < 480 For A533B steel. Transition temp. region
$K_{Id} = 15.5(CVNE)^{0.375}$		
$K_{Id} = 2 \times 10^{-3} P_f$	N.M.A.B. (1976)	Instrumented CVN. Transition temp. region low-med strength steels.

Where K_{Ic} is in MPa $m^{1/2}$, and Yield and E in MPa and CVNE in J

APPENDIX III

EQUIPMENT

CHARPY IMPACT MACHINE
Mouton Pendule No. 364 30 kw 4-1926 U of A # 00 42036

STRAIN GAUGES
Two double element semi-conductor

BRIDGE AMPLIFICATION MODULE
Intertechnology BAM-1 # 040246 U of A # 0116319

ACCELEROMETER
Endevco force-accelerometer Model 2224 U of A # 00 42150

AMPLIFIER
Endevco shock amplifier Model 2718A U of A # 00 42138

FILTER
Krohn-Hite dual filter Model 3342

DISPLACEMENT TRANSDUCER
Lohet Hall-effect displacement transducer Model 91SS12-2 Micro 2023
Magnet 106 MG10

POWER SUPPLY
Hewlett-Packard 12 volt power supply Model 6214A U of A # 00 42733

OSCILLOSCOPE
Hewlett-Packard four-channel oscilloscope Model 141B
1421A time base
1404A four-channel amplifier

CAMERA
Tektronix series 125 Polaroid camera

PROVING RING
Morehouse #4006 U of A # 00 42082

EXTENSOMETER
Starrett No. 657

APPENDIX IV

STEELS SPECIFICATIONS AND SPECIMEN ORIENTATION

The steels listed below were chosen (from those produced under University of Alberta Research Contract No. 59-0103) to provide a wide range of Charpy V-notch energies when tested at room temperature (20^{0}). One exception was ASTM A516 which was included to lie between energy levels of 30 J and 100 J. Although ASTM A516 specimen orientation is stated as L-T, it is possible that another orientation was erroneously produced in the specimens. This would account for the test results showing two distinct levels of energy absorbed, one at 30 J and the other at 80 J. The other exception was TT StE 26 which is a structural steel made in Germany. The specimens of this steel were also made in Germany and originally sent to the university for comparison to local steels.

TT St E 26, 20 mm PLATE, NORMALIZED

MELT (%) C = 0.08
Si = 0.24
Mn = 1.27
P < 0.025
S < 0.01
V < 0.05
Nb < 0.05

YIELD = 320 MPa UTS = 430 MPa
SPECIMEN ORIENTATION L-T

50A - CSA G40.21, ANGLE, AS ROLLED, 86 Rb

REQ. (%) C = 0.2
Mn = 0.75 - 1.35
P = 0.03
S = 0.04
Si = 0.15 - 0.40
Cu = 0.20 - 0.60
Ni = 0.90
Cr = 0.70

YIELD = 421 MPa UTS = 580 MPa % EL = 40
SPECIMEN ORIENTATION L-T

50T - CSA G40.21, PLATE, AS ROLLED, 69 Rb

REQ. (%), C = 0.22
Mn = 0.8 - 1.5
P = 0.03
S = 0.04
Si = 0.15 - 0.40

YIELD = 279 MPa UTS = 447 MPa % EL = 45

SPECIMEN ORIENTATION L-T

ASTM A516 GR 70, 13mm PLATE

MELT (%), C = 0.17
Mn = 0.15 - 1.17
P = 0.18
S = 0.02 - 0.03
Si = 0.24 - 0.26

YIELD = 381 MPa UTS = 550 MPa % EL = 26

SPECIMEN ORIENTATION L-T

AISI 8620 - 15.2 cm BAR, HOT ROLLED - STRESS RELIEVED, 88 RB 7 Rc

MELT (%), C = 0.20
Mn = 0.79
P = 0.014
S = 0.019
Si = 0.24
Cr = 0.58
Mo = 0.16
Ni = 0.45

YIELD = 358 MPa UTS = 574 MPa % EL = 30.2

SPECIMEN ORIENTATION L-R

AISI 4140 - 15.2 mm BAR, HOT ROLLED - STRESS RELIEVED, 22 Rc

MELT (%), C = 0.39
Mn = 0.79
P = 0.018
S = 0.016
Si = 0.25
Cr = 0.83
Mo = 0.16

YIELD = 1031 MPa UTS = 1073 MPa % EL = 19.1

SPECIMEN ORIENTATION L-R

AISI 4340 - 15.2 mm BAR, HOT ROLLED - STRESS RELIEVED, 27 Rc

MELT (%), C = 0.38
Mn = 0.62
P = 0.009
S = 0.016
Si = 0.27
Cr = 0.71
Mo = 0.21
Ni = 1.68

YIELD = 922 MPa UTS = 1003 MPa % EL = 22

SPECIMEN ORIENTATION L-R

CHT-100 - PLATE, AS ROLLED, 255 BH

REQ. (%), C = 0.16
Mn = 1.3
P = 0.015
S = 0.02
Si = 0.28
Mo = 0.23
V = 0.04
Ti = 0.02
Al = 0.06
B = 0.001

YIELD = minimum 690 MPa UTS = minimum 792 MPa

SPECIMEN ORIENTATION L-T

APPENDIX V

LOAD-TIME AND DISPLACEMENT-TIME OSCILLOSCOPE TRACES OF CVN IMPACT TESTS

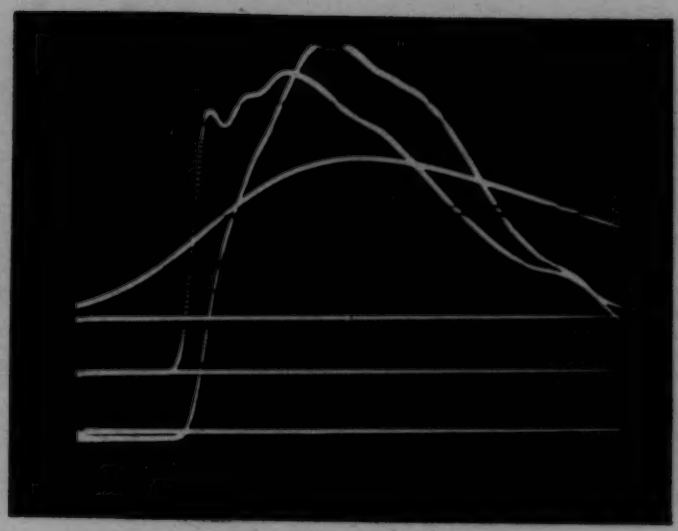

UPPER TRACE = DISPLACEMENT
(HALL-EFFECT TRANSDUCER)

MIDDLE TRACE = LOAN
(STRAIN GUAGES)

LOWER TRACE = LOAD
(ACCELEROMETER)

EXAMPLE OF IMPACT TEST SHOWING A QUASI-YIELD POINT
IN THE STRAIN GAUGE TRACE OF LOAD FOR AISI 8620 STEEL.

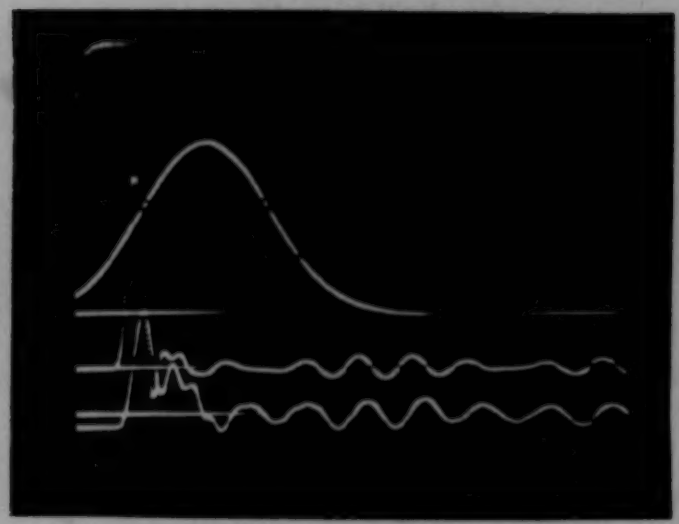

UPPER TRACE = DISPLACEMENT
(HALL-EFFECT TRANSDUCER)

MIDDLE TRACE = LOAD
(STRAIN GAUGES)

LOWER TRACE = LOAD
(ACCELEROMETER)

EXAMPLE OF IMPACT TEST SHOWING RINGING AT 900 Hz FOR AISI 4340 STEEL.